International Journal of Pharmaceutics 667 (2024) 124849

Contents lists available at ScienceDirect

International Journal of Pharmaceutics

journal homepage: www.elsevier.com/locate/ijpharm

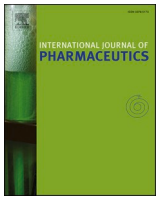

A microfluidic *in vitro* method predicting the fate of peptide drugs after subcutaneous administration

Marcus Wanselius [a], Susanna Abrahmsén-Alami [b], Belal I. Hanafy [c], Mariarosa Mazza [c], Per Hansson [a,*]

[a] Department of Medicinal Chemistry, Uppsala University, BMC P.O. Box 574, SE-751 23, Uppsala, Sweden
[b] Innovation Strategy & External Liaison. Pharmaceutical Technology & Development, Operations, AstraZeneca, Gothenburg, Sweden
[c] Advanced Drug Delivery, Pharmaceutical Sciences, BioPharmaceuticals R&D, AstraZeneca Cambridge, United Kingdom

ARTICLE INFO

Keywords:
Microfluidics
Microgel
Subcutaneous
In vitro method
SCISSOR
Polyelectrolyte
Peptide
Protein
Extracellular matrix (ECM)
Interstitial fluid (ISF)

ABSTRACT

For many biopharmaceuticals, subcutaneous (sc) administration is the only viable route. However, there is no *in vitro* method available accurately predicting the absorption profiles of subcutaneously injected pharmaceuticals. In this work, we show that a recently developed microfluidics method for interaction studies (MIS) has the potential to be useful in this respect. The method utilises the responsiveness of polyelectrolyte microgel networks to oppositely charged molecules as a means to monitor the interaction between peptides and hyaluronic acid (HA), a major constituent of the subcutaneous extracellular matrix. We use the method to determine parameters describing the strength of interaction between peptide and HA as well as the peptide's aggregation tendency and transport properties in HA networks. The results from MIS studies of the peptide drugs exenatide, pramlintide, vancomycin, polymyxin B, lanreotide, MEDI7219 and AZD2820 are compared with results from measurements with the commercially available SCISSOR system and *in vivo* absorption and bioavailability data from the literature. We show that both MIS and SCISSOR reveal differences in the peptides' diffusivity and tendency to aggregate in the presence of HA. We show that MIS is particularly good at discriminating between peptides forming aggregates stabilised by non-electrostatic forces in the presence of HA, and peptides forming complexes stabilised by electrostatic interactions with HA. The method provides two parameters that can be used to quantify the peptides' aggregation tendency, the one describing the peptide packing density in complexes with HA and the other the apparent diffusivity upon release in a medium of physiological ionic strength and pH. The order of the peptides when ranked by increasing binding strength at pH 7.4 determined with MIS is shown to be in agreement with the order when ranked by the apparent 1st order absorption rate constant (k_a) after sc administration in humans: lanreotide (Autogel) < exenatide (IRF) < AZD2820 < pramlintide < lanreotide (IRF) (IRF: Immediate release formulation). A correlation is found between the 1st order release rate constant determined with SCISSOR and k_a for lanreotide (Autogel), exenatide and AZD2820. A mechanism relating the magnitude of k_a to the peptides' charge is proposed.

1. Introduction

Subcutaneous (sc) administration is suitable for biopharmaceuticals ranging from small peptides up to large monoclonal antibodies. The sc route enables the drug to reach systemic circulation avoiding first-pass metabolism and degradation in the gastrointestinal tract and offers a more patient-centric route of administration for many therapies including higher doses and volumes (Stevenson et al., 2024). In comparison to intravenous (iv) administration, the sc route is suitable for self-administration by patients and for long-acting sustained-release (Bittner et al., 2018). However the bioavailability of drugs is lower after sc administration than after iv administration and more information is needed regarding the fate of drugs, as well as the formulations, after sc injection, before being absorbed into plasma (Fathallah and Balu-Iyer, 2015; Mach et al., 2011; Milewski et al., 2015; Collins et al., 2020; Kagan et al., 2012; Richter et al., 2012; Richter and Jacobsen, 2014). We are especially lacking sufficient understanding of the interaction between the injected drug-containing formulation and the extracellular

* Corresponding author at: Department of Medicinal Chemistry, Uppsala University, BMC P.O. Box 574, SE-751 23, Uppsala, Sweden.
E-mail address: per.hansson@ilk.uu.se (P. Hansson).

https://doi.org/10.1016/j.ijpharm.2024.124849
Received 28 June 2024; Received in revised form 14 October 2024; Accepted 18 October 2024
Available online 24 October 2024

matrix, and its effect on drug aggregation and mass transport (Kinnunen and Mrsny, 2014). This knowledge gap and the goal to reduce, replace, reuse, rehabilitate, and refine animal studies have created a need for *in vitro* and *ex vivo* methods with the ability to predict the behaviour of subcutaneously injected pharmaceuticals (Collins et al., 2017; Sánchez-Félix et al., 2020; Viola et al., 2018). This has resulted in *in vitro* models trying to emulate the mesh structure of the subcutaneous tissue as well as *ex vivo* models utilizing human skin biopsies (Bender et al., 2022; Bock et al., 2020; Jensen et al., 2016; Leung et al., 2017; Kožák et al., 2021). Other methods focus on capturing the effect of the interaction with hyaluronic acid and chondroitin sulphate, the most abundant polyelectrolytes in the interstitial fluid (ISF) in sc tissue (Kinnunen et al., 2015; Lou and Hageman, 2022). Electrostatic interactions with these negatively charged polymers are believed to affect the transport and aggregation behaviour of oppositely charged peptide and protein drugs (Kinnunen and Mrsny, 2014). The commercially available SubCutaneous Injection Site Simulator (SCISSOR), first described by Kinnunen et al., is an instrument designed to mimic the absorption of drugs by blood capillaries and lymphatic vessels after sc injection (Kinnunen et al., 2015; Thati et al., 2020; Lou et al., 2021; Mertz et al., 2019; Song et al., 2019; Bown et al., 2018). In the original version, formulations were injected into a solution of hyaluronic acid in a physiologically relevant buffer, and the rate of diffusive mass transfer to a receiver compartment, via a porous membrane, was monitored. SCISSOR has been used to establish *in vitro-in vivo* correlation (ivivc) between the *in vitro* release profiles and human *in vivo* absorption for a series of antibodies (Bown et al., 2018). Lou and Hageman (Lou and Hageman, 2022) developed a slightly different hyaluronic-based method (ESCAR) including separate compartments representing blood and lymph capillaries, with machine learning implemented. The method was used to establish a correlation between griseofulvin *in vitro* release rates and *in vivo* absorption in rats using *in vivo* PK data and two-compartment models gathered and developed by Chiang et al. (Chiang et al., 2019). More recently, Schöner et al. (Schöner et al., 2024) developed a well plate based method using solid collagen/HA-matrix proved to allow for the discrimination of different insulin formulations *in vitro* that claimed qualitative correlation to *in vivo* human data for some unspecified pharmacokinetic parameters. The work initiated by Torres-Teran (Torres-Terán et al., 2021; Torres-Terán et al., 2023) provides valuable input data for deeper understanding of the subcutaneous tissue to support translation through extensive characterisation of interstitial fluid of animals, non-human primates and humans.

In our lab we have developed extracellular matrix mimetic models (ECMM) based on either hyaluronic acid-based hydrogels or hydrogels containing a combination of collagen and hyaluronic acid (Rodler et al., 2024), and used them to study how peptides interact with and are transported through the matrix (Parlow et al., 2024). The aim is to investigate the different stages of subcutaneous administration and how the interactions affect the behaviour of a drug during different stages of the absorption process.

We recently developed a microfluidics-based method for investigations of the interaction between drugs and hyaluronic acid (Wanselius et al., 2022). The method is based on the principle that cross-linked hydrogels respond to the binding and release of charged molecules by changing volume. By observing spherical microgel networks, preferably by optical or confocal microscopy, it is possible to gain information about the strength of interaction with hyaluronic acid, the tendency for peptide aggregation in hyaluronic acid, and the peptide diffusivity in hyaluronic acid networks (Wanselius et al., 2022; Wanselius et al., 2023).

In this work, the microfluidics method is used to investigate the interaction between hyaluronic acid and seven different pharmaceutical peptides: pramlintide, exenatide, lanreotide, AZD2820, MEDI7210, polymyxin B, and vancomycin; see Table 1 for a description of peptide characteristics. Pramlintide, exenatide, and lanreotide are given subcutaneously to humans in the clinic; polymyxin B and vancomycin are today given intravenously in the clinic. More information about the peptides is provided as Supplementary material S1, including chemical structures (Figs. S1-S6). To benchmark the results, the peptides are also studied using SCISSOR. Finally, the MIS and SCISSOR results are compared with human *in vivo* data (absorption rate constant and bioavailability) determined after sc administration.

2. Materials and methods

2.1. Materials

Polydimethylsiloxane (PDMS) DowSyl Sylgard™ 184 elastomer and curing agent was procured from GA Lindberg ChemTech AB (Stockholm, SE). Picosurf™ 5 % in Novec™ 7500 was from Sphere fluidics (Cambridge, UK) and Novec™ 7500 (>99 %) was from 3 M (Saint Paul, MN, USA). Sodium hyaluronate (100–300 kDa) was purchased from Contipro a.s. (Dolní Dobrouč, CZ). The linker N-(2-aminoethyl) acrylamide hydrochloride (AEA) was from abcr GmbH (Karlsruhe, GE), and Spectra/Por® 6 RC-membrane (3.5 kDa cutoff) was from SpectrumLabs (Rancho Dominguez, CA). SUEX photoresist film was from DJ MicroLaminates (Sudbury, MA, USA), 2-propanol (ACS reagent) was purchased from Merck KGaA (Darmstadt, GE), and ethanol (99.7 %) was from Solveco (Rosersberg, SE). EDC (N-(3-dimethylaminopropoyl)-N'-ethylcarbodiimide hydrochloride was acquired from Acros Organics, (Geel, BE). mr-Dev 600 development solution was from micro resist technology GmbH (Berlin, GE). Glacial acetic acid (>99.7 %) was purchased from Thermo scientific, SE.

The following were all purchased from Sigma Aldrich, SE: Sodium acetate anhydrous (>99 %), Sigmacote®, sodium chloride (≥99 %), fluorescein isothiocyanate-dextran (FITC- dextran 4, 10, 40, 70 and 250 kDa), HOBt (1-hydroxybenzotriazole hydrate, ≥97.0 %), phosphate monobasic (ReagentPlus ≥ 99 %), sodium phosphate dibasic (ReagentPlus ≥ 99 %), acetonitrile (anhydrous 99.8 %), lithium phenyl-2,4,6-trimethylbenzoylphosphinate (LAP, 900889), sterile syringe filters (5 μm, Merck Millipore, Burlington, MA, US) and 1H,1H,2H,2H-perfluoro-1-octanol (≥97 %), sodium hydroxide (≥97 %).

Table 1
Molecular weight, isoelectric point (pI), pK_a, expected net charge, and diffusion coefficients in aqueous solutions (20 mM NaCl) at 298 K.

Peptide	Molecular weight (Da)	pI	pK_a	Expected net charge pH 4.5	Expected net charge pH 7.4	Peptide diffusion coefficient (D_0) (10^{-10} m^2/s)
Exenatide	4186	4.2[a]	N/A	0 (+2/+3)[b]	−2	3.2
Pramlintide	3943	10.2[c]	N/A	+3	+2	3.2
Lanreotide	1096	N/A	10.2	+2	+2	5.1
Vancomycin	1485	8.4[d]	N/A	(+2)	(+1)	4.4
Polymyxin B	1295	N/A	10.2	+5	+5	4.7
MEDI7219	4352	3.8	N/A	−3	−6	3.2
AZD2820	1057	N/A	11 & 6	+2	+1	5.2

a) Ref. (Skovgaard et al., 2006).
b) Net charge ~ 0 expected in solution while + 2 or + 3 in the more acidic gel environment provided by carboxylic acid groups on hyaluronic acid.
c) Ref. (Dunning et al., 2019).
d) Ref. (Johnson and Yalkowsky, 2006).

Photoresist S1813, Microposit™ 351 developer, H_3PO_4, CO_3COOH, and HNO_3 were all lab grade and provided by the Ångström Microstructure laboratory, Uppsala. Hyaluronic acid-based extracellular matrix was purchased from Pion inc., UK, and Carbonate based buffered medium was provided by AstraZeneca Cambridge, UK. The peptides exenatide, pramlintide, MEDI7219 and AZD2820 were all provided by AstraZeneca Gothenburg, SE. Lanreotide was purchased from BCN Peptides, ES. Vancomycin hydrochloride (PHR1732 Lot: LRAC0718) was purchased from Sigma Aldrich, SE, and polymyxin B sulfate salt (TCL P1923, Lot:L2V4M-DR) was ordered from VWR, SE.

2.2. Peptide diffusivity measurements

Peptide diffusion coefficients in water containing 20 mM NaCl at 295 K was determined by means of dynamic light scattering using a Nanotrac Wave II from Microtrac (Pennsylvania, USA). Diffusion coefficients were successfully acquired for vancomycin, polymyxin B, lanreotide, AZD2820, and MEDI7219. For exenatide and pramlintide the measurements failed because of aggregation already at the lowest concentration required to obtain a measurable signal. The measured diffusion coefficients were plotted *vs*. the inverse molar mass of the peptides (Fig. S7) and the diffusion coefficient (D_0) of all peptides were determined by means of a linear equation fitted to the data points. The result is presented in Table 1.

2.3. Fabrication of microfluidic chip for droplet production and interaction studies

The manufacturing of the Microfluidic chips for Droplet Production (MDP) was done with standard soft lithography techniques and using PDMS as chip material; the manufacturing process has been described earlier in detail by Wanselius et al. (Wanselius et al., 2022). The Microfluidic Chip for Interaction Studies (MIS) was fabricated using wet etching techniques with glass and silicon wafers, as described elsewhere. (Wanselius et al., 2022).

2.4. Synthesis of hyaluronic acid-ethyl acrylamide derivative and production of microgels

The hyaluronic acid-ethyl acrylamide derivatives were synthesised as described by Shi et al. (Shi et al., 2017). Microgels were produced by the method described by Wanselius et al. (Wanselius et al., 2022).

2.5. Determination of microgel volume

The aqueous medium in the binding studies was either phosphate buffer (pH 7.4) containing sodium phosphate monobasic (7 mM) and sodium phosphate dibasic (3 mM), or acetate buffer (pH 4.5) containing sodium acetate (4.5 mM) and acetic acid (5.4 mM). The phosphate buffer will be denoted PB and the acetate buffer AcB. Small amounts of HCl were added to adjust the pH value. The release medium was PB (pH 7.4) with 0.15 M NaCl added. Image capture was performed with an Olympus BX51 microscope equipped with an UMPlanFI 5 × lens and an Olympus DP73 digital camera using the imaging software cellSens Dimension version 1.7.1 from the Olympus Corporation.

2.6. The microgel approach

Microgels can be used to probe interactions between polyelectrolytes and protein/peptide drugs (Wanselius et al., 2022; Eichenbaum et al., 1999; Bysell et al., 2010; Bysell et al., 2009; Hansson et al., 2012; Li et al., 2010; Hansson, 2020). The approach is based on the principle that charged microgel networks respond to binding and release of oppositely charged species by deswelling and swelling, respectively. The response can be quantified by determining the change in microgel volume. The volume change is a result of ion exchange between peptides and simple monovalent counterions to the fixed network charges, a process accompanied by water being exchanged with the surroundings. For a given polymer network, the response typically increases in magnitude with decreasing ionic strength of the solution and increasing peptide charge.

The relevance of the method for subcutaneous administration is illustrated in Fig. 1. During administration, the injected formulation spreads in cracks formed as the extracellular matrix (ECM) between fat lobules is ripped apart by the injection pressure (Comely and Fleck, 2011) (cartoon to the left). Depending on the volume injected, a bolus 1 – 2 cm in width is created, containing also the blood capillaries through which most of the drugs will be absorbed. The process can roughly be divided into two steps: (1) Peptide release from the formulation into ECM, and (2) Diffusion of peptide through ECM to capillaries. Because the formulation occupies a large volume fraction in the bolus, its composition will affect the average composition of the interstitial fluid in that region, including ionic strength and pH, and thereby the strength of interaction between the peptide and HA and other macromolecules in the extracellular matrix. The interactions are expected to be particularly strong for formulations prepared at low ionic strength, where the binding to HA may lead to peptide aggregation or the formation of electrostatically stabilised peptide-HA complexes affecting the bioavailability and the drug release rate (*step 1*). When released, the peptide will diffuse through the ECM (*step 2*). With time, the composition of the medium will approach the physiological composition of the surrounding tissue. In the microgel experiments in this work (Fig. 1 top right), spherical microgels are first exposed to a peptide formulation at low ionic strength. Cationic peptides will spontaneously accumulate in the microgels. This process, where the peptide penetrates and interacts with the HA network, resembles *step 1*. Changing the medium to a constantly renewed peptide-free solution with physiological ionic strength and pH, acting as a sink, will trigger the release of peptide. Typically, at intermediate stages during release, a complex-depleted shell develops outside a core of “undissolved” complexes (Fig. 1 bottom right). The diffusive transport through the shell resembles *step 2* where the peptide diffuses through HA in the ECM.

2.7. MIS experiments

We investigated interactions between peptide drugs and HA microgel network by means of the recently developed MIS (Microfluidic chip for Interaction Studies) method, schematically illustrated in Fig. 2. For a detailed description and evaluation of MIS, see Wanselius et al. (Wanselius et al., 2022). Microgels confined to hydrodynamic traps on the chip were monitored while exposed to a flow of peptide solution (binding/loading) or saline buffer solution (release). Solutions were pumped into the microfluidic chip through inlets (1) and (2) by means of pressure pump OB1 MK3 including the OB1 MK3 + flow controller with associated MFS flow sensors and a MUX 12 distributor all from Elveflow (Paris, FR). Masterflex tubings (EW-06417–11) of inner diameter 300 μm were used to connect the flow controller and accessories to MIS. The flow was controlled by the software ESI also from Elveflow. The MUX 12 distributor was used to change between drug solution, PB, AcB, and the release medium. Inlet (1) was only used to gradually change the peptide concentration and ionic strength during experiments by varying the flow rates of two solutions of different concentration entering via inlet (1) and (2), respectively. 16 microgels were simultaneously monitored and recorded by means of Olympus BX51 microscope.

In a typical experiment, the chip was initially flushed with PB or AcB before loading the traps with microgels, one in each trap, using a syringe connected via tubing to inlet (4). We used spherical HA microgels in the size range 100–200 μm. Peptide binding and release were studied in sequence by first flowing a peptide solution of a certain concentration at low ionic strength through the chip and subsequently the release medium mimicking the pH and ionic strength *in vivo* (PB; pH 7.4; 150 mM NaCl) without any peptide in it. During both steps, microscopy images

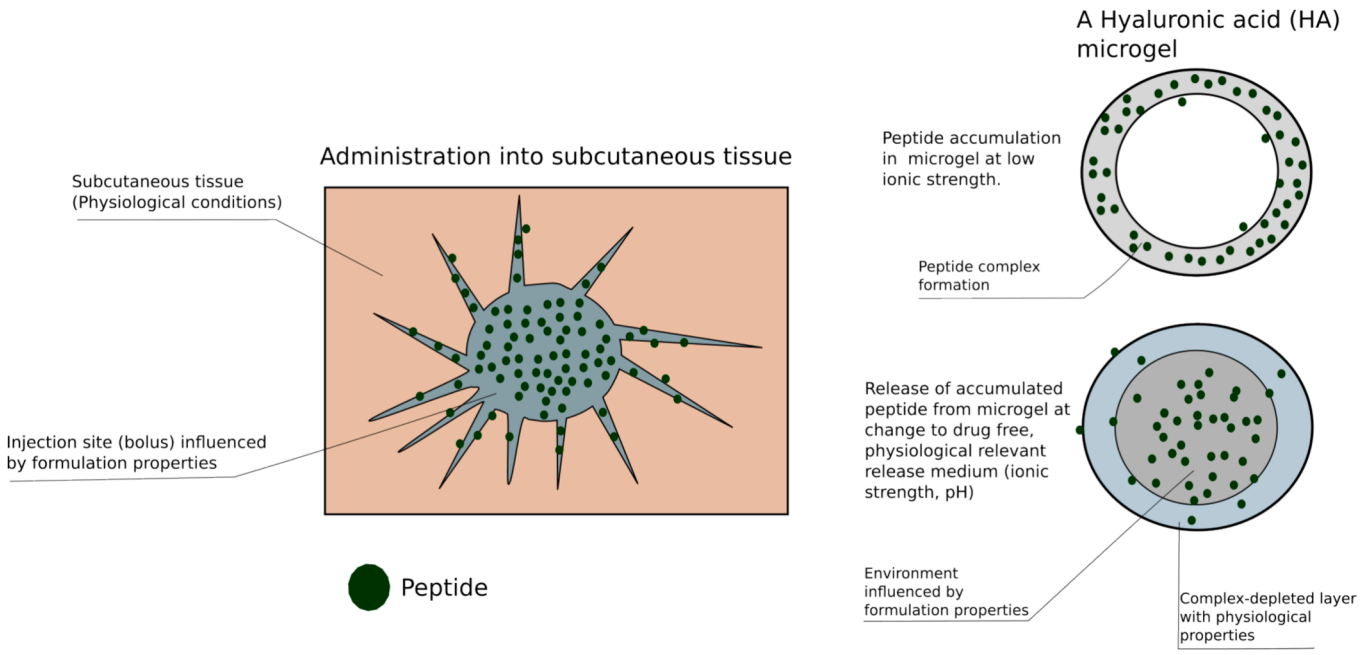

Fig. 1. Illustration to show the *in vivo* relevance of the microfluidic method used in this work.

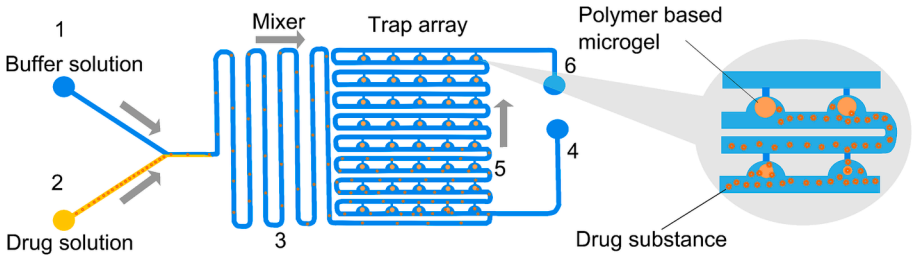

Fig. 2. Illustration (reused with permission from Wanselius et al. (Wanselius et al., 2022)) of a microfluidic chip used for interaction studies (MIS) not according to scale; arrows indicate the flow direction. (1) Inlet for solvent, (2) inlet for solution of drug molecule, (3) mixer for complete mixing of the solvent and stock solution, (4) inlet for microgels, (5) 96 single-microgel traps of 200 μm diameter, (6) outlet for liquid.

were taken in order to monitor the evolution of the microgels. The volume of the microgels at different time points was determined from the images by assuming a spherical microgel shape. If nothing else is specified, the volume flow rate through the chip was 200 μl/min. The corresponding apparent flow velocity through the traps has been determined to 12 ± 2 cm/s in previous works using the MIS, which is within a range where the apparent stagnant layer thickness and the swelling of the studied microgels are insensitive to small variations of the flow rate (Wanselius et al., 2022). All experiments were performed at 34C° by using a Ibidi heating system (Ibidi, GE) with an incubator chamber adapted for perfusion experiments.

2.8. MIS data analysis

2.8.1. Binding

Equilibrium data will be presented as swelling isotherms, i.e., plots of V/V_0 *vs.* peptide concentration in the bulk liquid in contact with the microgels, where V is the actual gel volume and V_0 the volume in a peptide-free solution of otherwise identical composition. The shape of the swelling isotherm gives information about the nature of the interaction and the mechanism of binding. Highly cooperative peptide binding can give rise to a volume phase transition (VPT), characterised by a discontinuity in the swelling isotherm at a certain peptide concentration denoted the critical collapse concentration (CCC) (Hansson, 2020). For quantitative purposes, we will use two measures related to the "fully collapsed" state, which is the state of lowest microgel volume in the peptide solution: C_{pep}^{liq}, which is the concentration of peptide in the solution required to attain the fully collapsed state, and C_{pep}^{gel}, which is the concentration of peptide in the fully collapsed microgels, taken to be equal to MC_p^{gel}/Z, where M is the peptide's molar mass, C_p^{gel} is the molar concentration of fixed network charges in the microgel, and Z is the peptide's charge number. C_p^{gel} will be calculated from the collapse amplitude and the pre-determined HA concentration in the peptide-free microgel. The error introduced by assuming a peptide/network charge ratio (β) equal to unity should not be larger than ca. ± 10 %, based on previous results for similar systems (Jidheden and Hansson, 2016; Liang et al., 2019; Karabanova et al., 1995; Zezin et al., 2002; Kabanov et al., 2004).

The kinetics of the binding process also provides important information but is more difficult to quantify. Here we will only quantify the initial part of the binding process in order to discriminate between intra-particle and stagnant layer-controlled processes. We will do this by fitting the initial part of plots of microgel volume *vs.* time to the following equation derived for a stagnant layer controlled process, i.e., processes rate controlled by the mass transfer of peptide from the bulk liquid to the microgel via the "stagnant" layer surrounding the microgel (Wanselius et al., 2022; Wanselius et al., 2023; Ahnfelt et al., 2018; Al-Tikriti and Hansson, 2020):

$$\frac{V(t)}{V_0} = (1 - k_0(t - t_{lag}))^{3/2} \quad (1a)$$

$$k_0 = \frac{ShZCaD}{C_{p,0}^{gel} R_0^2} \quad (1b)$$

V is the actual microgel volume, V_0 is the microgel volume in the medium with no peptide present, t_{lag} is a "lag time" describing the time for the microgel to start responding to the release medium, Sh is the Sherwood number, C is the peptide concentration in the medium, D is the peptide diffusion coefficient in the medium, $C_{p,0}^{gel}$ is the concentration of fixed charges on the polymer network prior to binding, R_0 is the microgel radius in the peptide-free medium, and a is an empirical constant. Eq. (1) is based on the assumption that $V/V_0 = 1 - a\beta$, where β is the peptide to network charge ratio in the microgel. Previous work show that this is a good approximation for small β, and a is often close to 1 (Jidheden and Hansson, 2016; Karabanova et al., 1995; Zezin et al., 2002; Kabanov et al., 2004; Skobeleva et al., 2001). The "rate constant" k_0 determined from the fit will be used to calculate D, which will be compared with the diffusion coefficient of the peptide in water (D_0)

2.8.2. Release

A general theory describing the relationships between swelling rate and transport properties is presently not at hand. However, the microgel systems investigated in this paper displayed a core–shell partitioning during release. This is consistent with the "depletion layer " mechanism observed in related systems, in which a dense complex phase (core) gradually dissolves while maintaining a sharp boundary to the surrounding swollen and peptide-lean phase (shell) (Ahnfelt et al., 2018; Al-Tikriti and Hansson, 2020). Equations describing the swelling kinetics, when the diffusive transport of a monovalent drug through the shell is the overall rate controlling process, have been presented elsewhere (Al-Tikriti and Hansson, 2020). Because of the complication that the shell network swells gradually and deforms non-uniformly during the process, we were only able to derive approximate expressions valid at (quasi-) steady state. In the present case of multivalent peptides, the electrostatic interactions impose an additional difficulty. Here we present a simplified version of the previous model based on the following assumptions. (1) The swelling of the network at each distance r from the centre of the microgel is a linear function of the local charge ratio $\beta(r)$ between peptide and HA at distance r from the gel centre: $\frac{v_p(r)}{v_{150}} = 1 - a\beta(r)$, where $v_p(r)$ is the local volume per segment in the network and v_{150} is the corresponding quantity in a peptide-free network in equilibrium with 150 mM NaCl solution. (2) During release, the microgel consist of a concentrated core of peptide-HA complexes and a swollen shell. (3) At every point in time, the peptide concentration profile is the one corresponding to quasi-steady state in the shell. The profile is then determined by the peptide diffusion coefficient in the shell, the shell thickness, the peptide concentration in the shell at the core/shell border and the concentration at the microgel surface (assumed = 0). (4) The concentration of dissolved peptide in the shell in local equilibrium with the complexes in the core is KC_c, where K is a distribution constant and C_c is the peptide concentration in the core. Under those conditions, the microgel volume V is given by (Supplementary material S3):

$$\frac{V(t)}{V_{150}} = 1 - a\beta_t \quad (2)$$

where V_{150} is the volume of the peptide-free microgel in equilibrium with the release medium with 150 mM NaCl. The overall charge ratio β_t between peptide and HA at time t is given by:

$$t = \frac{R_1^2}{2KD}\left\{(\beta_t^{2/3} - 1) + \frac{R_1}{aR_0}\left((1 - a\beta_t)^{2/3} - (1 - a)^{2/3}\right)\right\} \quad (3)$$

where R_0 is the microgel radius of the peptide-free network ($\beta = 0$), and R_1 is the microgel radius when $\beta = 1$, assumed to correspond to the fully collapsed state.

2.9. SCISSOR experiments

We used the SCISSOR system from Sirius Analytical Ltd., now PION, UK, designed to mimic the injection of formulations into the subcutaneous tissue and subsequent steps, including drug transport through subcutaneous tissue and absorption by the circulatory system. The instrument has been described in detail by others (Kinnunen et al., 2015; Song et al., 2019; Bown et al., 2018). A schematic picture of the setup is shown in Fig. S8. Briefly, test formulations are injected via a syringe into a dialysis cartridge filled with 5 ml hyaluronic acid solution. The solution is in contact with 50 ml of carbonate buffered release medium (6.4 g NaCl, 0.09 g $MgCl_2{\cdot}6H_2O$, 0.4 g KCl, 0.2 g $CaCl_2$, 2.1 g $NaHCO_3$ and 0.2 g sodium azide per 1 l Milli-Q water) via two polycarbonate membranes (pore diameter: 5 μm). In our study, the temperature and pH were maintained at 34 °C and 7.4, respectively. Peptides were formulated by dissolving powder in 500 μl milliQ water and injected into the cartridge by means of 1 ml syringes with 16 mm 25G needles. Temperature, pH, and light transmittance were recorded every 5 s for the first 15 min, followed by every 30 s up to 6 h, and then finally every 1 min until the end of the experiment. Aliquots (50 or 100 μl) taken out from the release medium were analysed by measuring the absorption at wavelength 280 nm for exenatide, pramlintide, vancomycin, and AZD2820, and at 242 nm for polymyxin B and MEDI7219. The determined concentrations at each point of time were converted to the fraction of drug released to the medium and the result was presented as plots of fraction released *vs*. time. The volume removed from the release chamber when taking aliquots was not replaced or accounted for. A slight deviation from the "true" concentration when calculating fraction released are therefore expected, however this deviation is at the most 3 % after 24 h and was seen as negligible. For more details, see Supplementary materials S4.

2.10. SCISSOR data analysis

We considered the transfer of drug from the injected formulation to the release medium to involve three steps: (i) Dissolution or release of drug from the formulation (ii) Transport of drug through the HA-solution and (iii) Transport through the membrane. To model the initial release rate we distinguished between to cases. (1) The injected aqueous formulation formed a depot enclosed by the viscous HA-phase; the drug inside the formulation remained fully dissolved at all times. (2) The drug formed aggregates/precipitates in the depot in local equilibrium with dissolved drug molecules.

As shown in Supplementary material S5, case (1) leads to first order and case (2) to zero order release kinetics, but in both cases the initial slope k of the curve in a plot of fraction released *vs*. time can be written

$$k = \frac{AK'D}{LV} \quad (4)$$

A and L are area and thickness respectively of the liquid film between the injected depot and the membrane, V is the volume of the depot, and K' is a partition coefficient between the depot and the HA-solution. The "rate constant" k is proportional to the drug's diffusion coefficient (D) in the HA-solution. $K'D$ can be viewed as the apparent diffusivity. We will use k primarily to compare the release rates between different peptides. This is reasonable since A, L, and V will be approximately the same in all experiments. To see the expected order of magnitude of k, we put $A = 1$ cm^2, L=0.3 cm, V=1 cm^3, K'=1, and $D = 3 \times 10^{-10}$ m^2/s, the latter a typical value of the diffusion coefficient in water for the investigated peptides. From Eq. (4) we get $k = 2 \times 10^{-5}\ s^{-1} \approx 0.07\ h^{-1}$; $k/D \approx 7\ cm^{-2}$.

3. Results and discussion

3.1. MIS results

3.1.1. Equilibrium swelling isotherms

Fig. 3 shows the equilibrium-swelling ratio (V/V_0) of HA-microgels as a function of the peptide concentration in the aqueous solution flowing through the microfluidic chip. The solution contained 0.01 M PB or AcB to maintain the pH at 7.4 or 4.5, respectively. The swelling isotherms for exenatide (pH 4.5), vancomycin (pH 4.5/7.4), pramlintide (pH 4.5) and AZD2820 (pH 4.5/7.4) show that the interaction between peptide and HA was strong for positively charged peptides when the concentration in the solution was sufficiently high. The result is in agreement with previous studies showing that, at low ionic strength, multivalent molecules or amphiphilic molecules forming multivalent self-assemblies spontaneously accumulate in HA microgels (Wanselius et al., 2022; Wanselius et al., 2023). Fig. 4 (top) shows microscopy images of two HA microgels in equilibrium in a solution of 40 mg/ml AZD2820 (pH 7.4) representative of peptide-loaded microgels confined to traps on the microchip; for microscopy images of the other systems, see Figs. S9-S13. No data was obtained for pramlintide at pH 7.4 because precipitation in the solution occurred already at concentrations of around 0.2 mg/ml and the precipitate did not dissolve when the medium was changed to AcB (pH 4.5). For exenatide and vancomycin, the discontinuity in the swelling curve suggests that the microgels underwent a volume phase transition (VPT) at a critical collapse concentration (CCC) (Hansson, 2020; Matuso and Tanaka, 1988; Tanaka, 1978). Above that concentration, the volume ratio varied little with concentration. The behaviour is characteristic of molecules forming self-assemblies inside hydrogels of opposite charge to the molecule, often resulting in complexes with charge ratio β between the binding molecule and the network close to unity (Hansson et al., 2012; Al-Tikriti and Hansson, 2020; Khokhlov et al., 1992; Nilsson and Hansson, 2005;

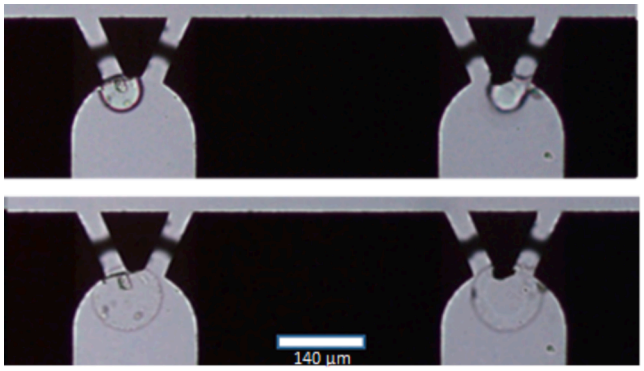

Fig. 4. Microscopy images of HA microgels fully collapsed in solution of 40.4 mg/ml AZD2820 (top), and after release in PB 150 mM NaCl (bottom).

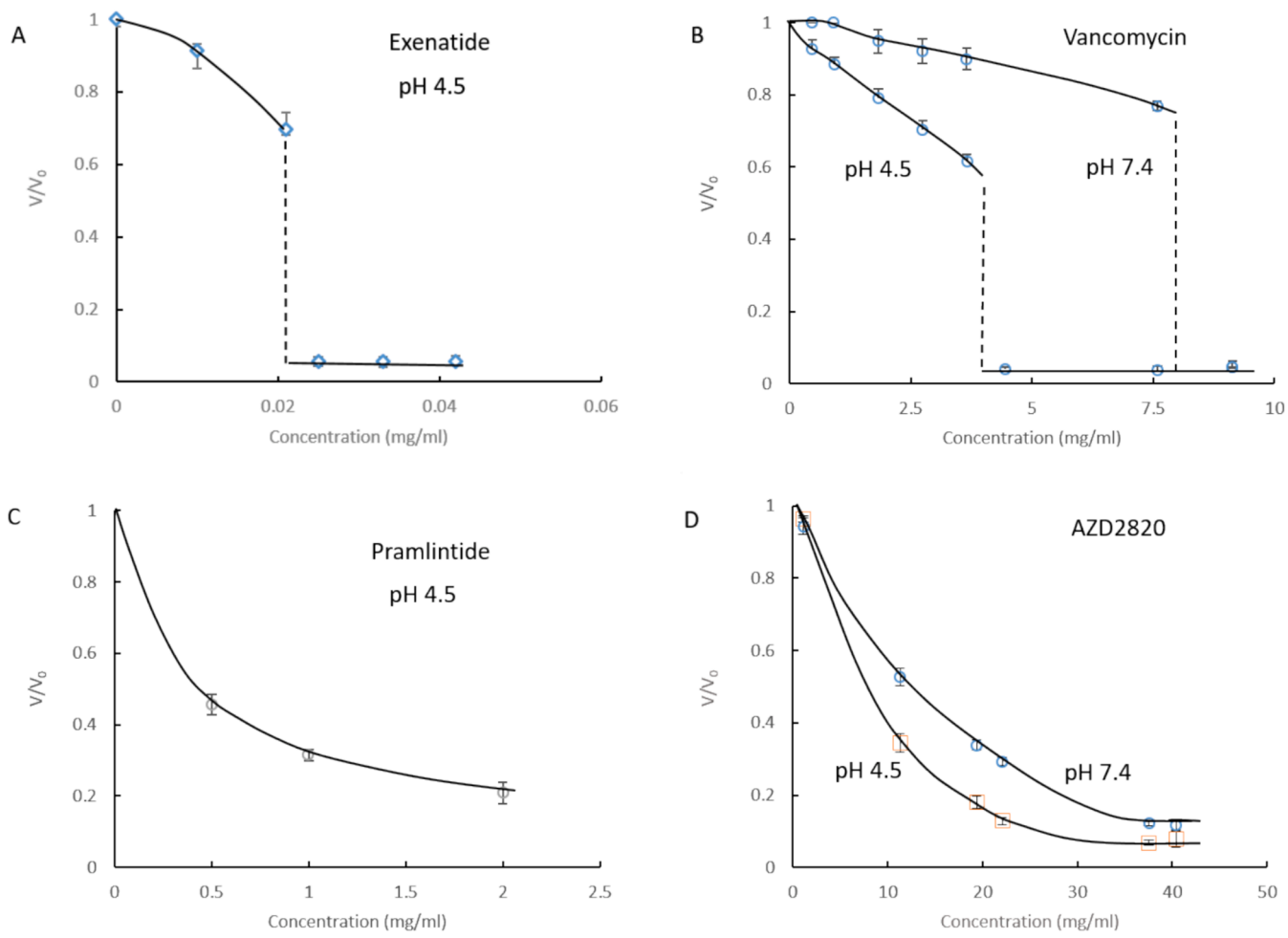

Fig. 3. Equilibrium swelling of HA-gels in peptide solutions showing the volume ratio V/V_0 plotted *vs.* the concentration of peptide in the solution in equilibrium with the microgels. V is the actual gel volume and V_0 is the volume in peptide-free solution of otherwise identical composition. Lines are just guides to the eye.

Nilsson and Hansson, 2008; Sasaki et al., 2001; Al-Tikriti and Hansson, 2022). For vancomycin at pH 7.4, where the peptide charge is +1, the volume change below CCC was substantially larger than that induced by monomeric univalent salt ions (Wanselius et al., 2022). This is a clear indication that the peptide formed self-assemblies already in that concentration range. At pH 4.5, where the peptide charge is +2, the volume change prior to CCC was even larger, but in this case the effect is difficult to distinguish from that expected from ion exchange between monovalent and divalent ions. For pramlintide and AZD2820 the swelling isotherms displayed no VPT. Instead, the microgel volume decreased monotonically with increasing peptide concentration. Polymyxin B and lanreotide induced substantial volume changes, but for the former we were not able to confirm a VPT because the microgels were fully collapsed at all concentrations investigated, and for the latter it was not possible to determine the equilibrium state because of the very slow volume response (see below). MEDI7219 (Fig. S14) and exenatide (pH 7.4) induced negligible volume changes, as expected because of their negative charge.

Table 2 shows the determined CCC:s together with the peptide concentration in the fully collapsed microgels C_{pep}^{gel}. It is clear that both parameter values varied greatly between the peptides, showing that the method can reveal differences in interaction strength as well as peptide packing density.

3.1.2. Binding/deswelling kinetics

Fig. 5 shows how the volume of the HA microgels evolved with time during exposure to peptide solutions of different concentration and pH; the microgel volume V has been normalised with the volume V_0 in the peptide-free medium. Fig. S15 shows an enlarged view at small times. The deswelling behaviour can be divided into two categories. For exenatide (C > CCC), vancomycin (C > CCC) and AZD2820, the volume gradually relaxed down to the equilibrium value and seemed to follow one single mechanism. The behaviour is similar to that observed earlier in systems where the binding species (protein/surfactant micelle) formed complexes with the network chains stabilized mainly by electrostatic forces. The other systems displayed a two-step process in which the volume change was fast the first 1–2 min but then abruptly changed to a much slower rate. The break point in the curves occurred at a lower volume ratio the higher the peptide concentration in the solution. A comparison between the curve for exenatide measured at 0.26 mg/ml (pH 4.5) and that for lanreotide at 0.275 mg/ml (pH 7.4) illustrates the difference between the two types deswelling pattern. Whereas the exenatide curve reaches the fully collapsed equilibrium state ($V/V_0 \approx 0.06$) after ca. 7 min, the lanreotide curve enters a very slow relaxation phase at $V/V_0 \approx 0.9$ already after ca. 2 min, and reaches $V/V_0 \approx 0.2$ after ca. 2.5 h. The latter behaviour is similar to what has been observed earlier for proteins aggregating inside microgels (Andersson and Hansson, 2018; Johansson et al., 2009).

To get information about the rate controlling process during the initial part of the binding process we fitted Eq. (1) to the initial part of the deswelling curves (Fig. S15). The result is presented in Table 2 as the mean value of the apparent diffusion coefficient in water (aD) determined at different concentrations. Since $a \sim 1$ (see above) and since we are only comparing orders of magnitude, we will treat aD as the apparent diffusivity in the aqueous stagnant layer to be compared with D_0, the peptide's actual diffusivity in water (Table 1). For exenatide and pramlintide the determined diffusivities were of the same order of magnitude as D_0, indicating that the initial deswelling rate was largely influenced by peptide mass transfer in the liquid surrounding the microgels (stagnant layer control). Previous investigations show that this is typical of microgels undergoing VPT during loading, where the binding molecules and the network form a dense complex phase ("shell") in the outer parts of the microgels, growing in thickness at the expense of the swollen core phase (Ahnfelt et al., 2018; Al-Tikriti and Hansson, 2020; Nilsson and Hansson, 2005; Andersson et al., 2005; Nilsson and Hansson, 2007). For the other peptides the diffusivities were 1–2 orders of magnitude smaller than D_0, ruling out a process rate controlled by stagnant layer diffusion of peptide monomers. Lanreotide (Pouget et al., 2010) and vancomycin (Phillips-Jones et al., 2017) have been proposed to form dimers and dimers/hexamers, respectively, in aqueous solutions. However, since the apparent diffusivities are smaller than expected also for such self-assemblies, we conclude that the deswelling rate is controlled by intra particle processes.

3.1.3. Release/swelling kinetics

Fig. 6 shows the swelling response of the microgels in the release medium (PB, 150 mM NaCl, pH 7.4). The plots show the ratio V/V_{150} as a function time, where V_{150} is the volume of the peptide-free microgel in equilibrium with the release medium. The experiments were made with the peptide-loaded microgels resulting from the binding experiments in Figs. 3 and 5. For the microgels with high initial peptide load, the swelling ratio increased when exposed to the release medium, as expected upon release when the volume of the peptide-loaded microgel is smaller than for the peptide free microgel in the release medium. The reason why some of the swelling curves for vancomycin, pramlintide and AZD2820 decreased during release is because the peptide load was so small that the microgel volume in the loading medium (low ionic strength) was larger than that in the peptide-free release medium (high ionic strength). Note also that the volume ratio increases more than two times when normalizing with the volume of the peptide-free microgel at ionic strength 150 mM (V_{150}) instead of the volume in the peptide-free medium in the binding experiment (V_0).

To facilitate comparisons between the behaviours of the different peptides at short times, we have plotted in Fig. 7 swelling curves on a

Table 2
Parameters determined with MIS and SCISSOR at 34 °C.

Peptide	MIS						SCISSOR		
	CCC (mg/ml)	C_{pep}^{gel}(g/ml) pH 4.5	C_{pep}^{gel}(g/ml) pH 7.4	aD (load.) (10^{-10} m^2/s)	KD (rel.) (10^{-10} m^2/s)	$\frac{V_\infty}{V_{150}}$	Total fract. rel.	k (h^{-1})	k/D_0 (cm^{-2})
Exenatide	0.023[a]	1.0	–	2[a]	0.11	0.85	0.8	0.029	4.8
Vancomycin	4[a] 9[b]	0.57	1.1	0.05[a] 0.07[b]	0.010	0.4	0.9	0.040	3.6
Polymyxin B	–	0.11	0.080	0.03[a] 0.03[b]	0.0075	0.9	1	0.076	5.9
Pramlintide	–	0.22	–	1[a]	0.0070	0.57	≈ 0	–	–
Lanreotide	–	–	0.080	0.1[b]	0.0045	(0.5)[c]	0.4	0.0025	0.18
AZD2820	–	0.27	0.31	0.02[a] 1[b]	0.031	0.9	1	0.10	7.3
MEDI7219	–	–	–	–	–	.	0.7	0.036	3.1

a) Determined at pH 4.5.
b) Determined at pH 7.4.
c) Highest value measured.

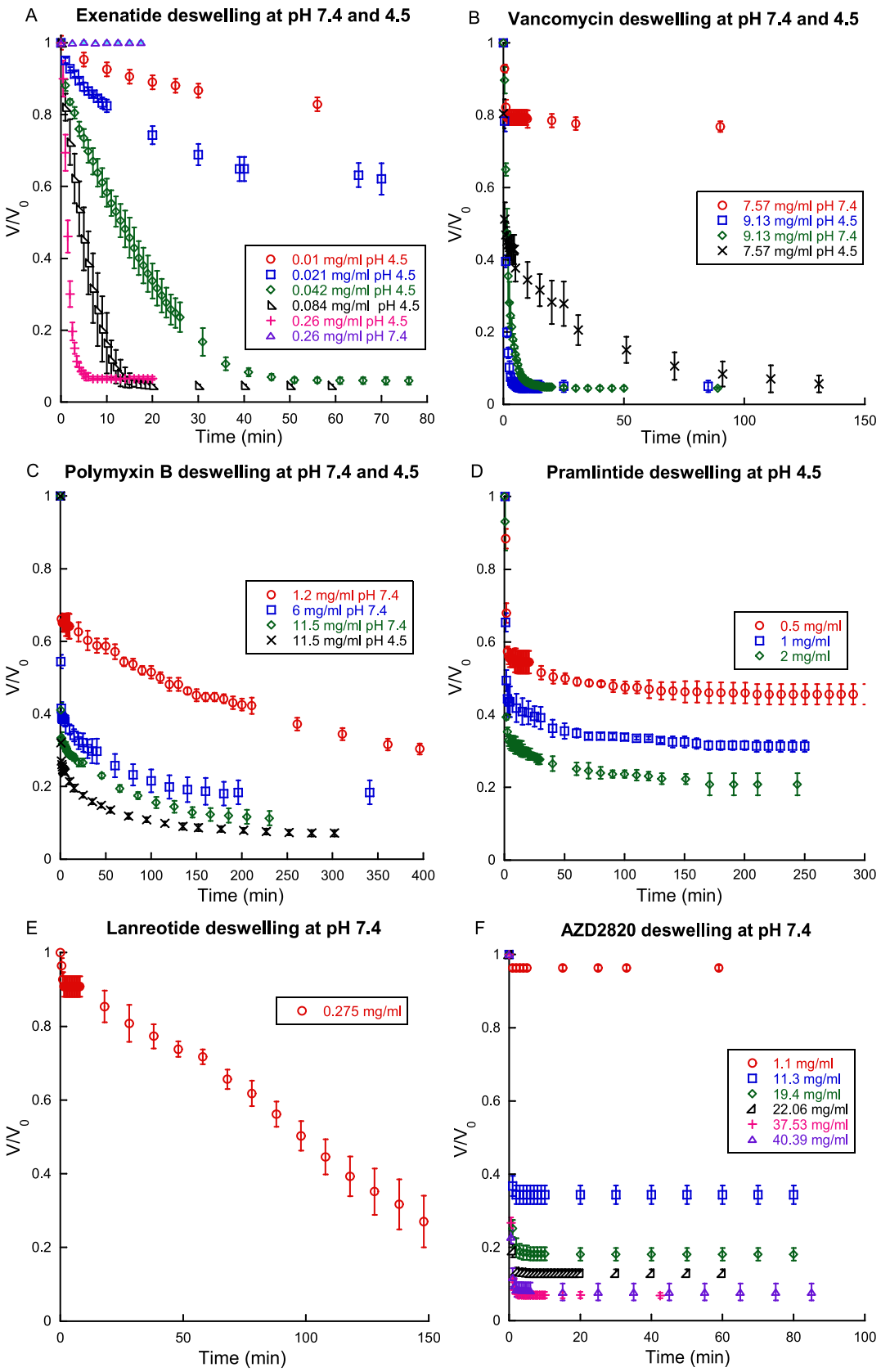

Fig. 5. Deswelling/binding kinetics. The microgel volume ratio V/V_0 plotted *vs.* time during exposure of microgels to solutions with peptide concentration and pH as indicated. V is the actual gel volume and V_0 is the volume in peptide-free solution of otherwise identical composition.

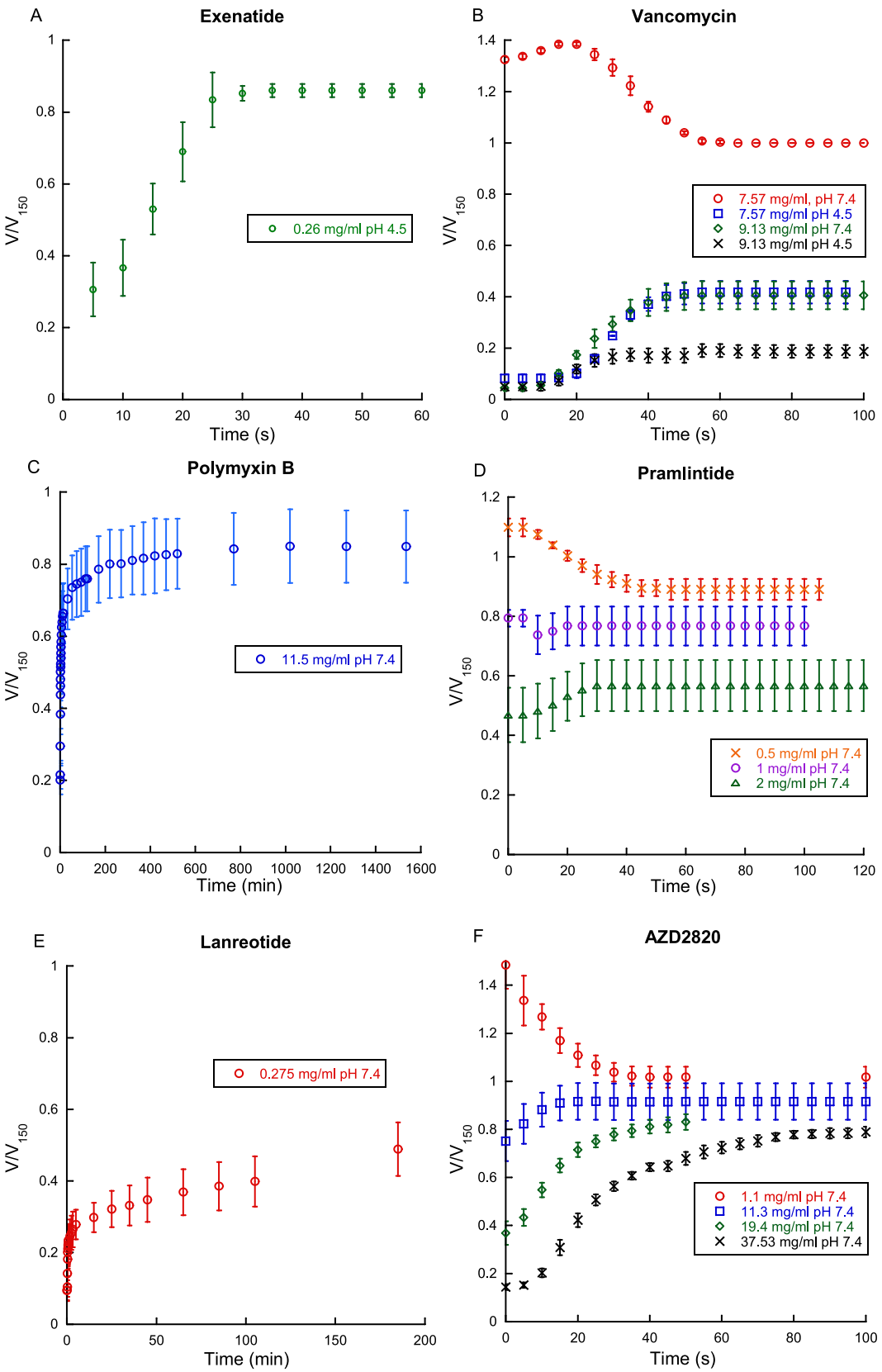

Fig. 6. Swelling/release kinetics. The microgel volume ratio V/V_{150} plotted *vs*. time in the release medium (PB, pH 7.4, 150 mM NaCl). V is the actual gel volume and V_{150} is the volume in the peptide-free release medium. The microgels were loaded in solutions with peptide concentration and pH as indicated in the legends; *cf*. Fig. 5.

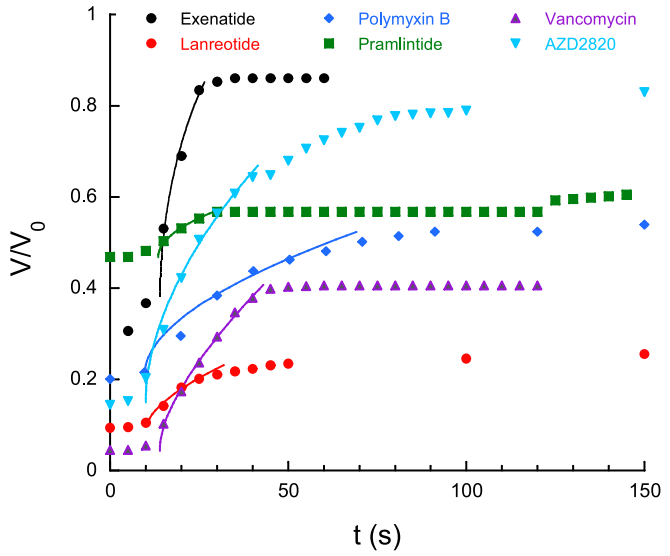

Fig. 7. Volume change of HA microgels upon peptide release. Initial swelling response fitted with eqs. (2)-(3) to acquire *DK* values. Release medium: PB (150 mM NaCl, pH 7.4).

common time scale in the same graph (error bars omitted). The data was taken from Fig. 6; for vancomycin, pramlintide and AZD2820 we included only one curve each for microgels fully loaded before exposed to the release medium. Fig. 7 shows that, after a short lag period, the swelling rapidly increased during the first 1–2 min but then levelled off at swelling ratios that were highly system specific. A comparison with the full plots in Fig. 6 shows that for all systems in Fig. 7, except polymyxin B and lanreotide, the final swelling ratio was reached after 150 s. However, none of the systems fully recovered the microgel volume in the peptide-free release medium; the determined final swelling ratios V_∞/V_{150} varied between 0.4 and 0.9 (Table 2). Exenatide (Hudson and Andersen, 2004; Benet et al., 2021), pramlintide (Cort et al., 2009; Brunzell et al., 2024) and lanreotide (Pouget et al., 2010; Pieri et al., 2022) have well documented aggregation properties that may have contributed to the effect, and exenatide aggregates were actually observed in the microchip at the concentration 0.26 mg/ml in PB (Fig. S9). For polymyxin B, which is not expected to aggregate, the extended swelling period is more likely related to strong electrostatic interactions with the HA because of its high positive charge.

In order to relate the swelling rates to release rates we fitted the release model in eqs. (2) – (3) to the initial part of the swelling curves in Fig. 7 (solid curves). This allowed us to determine the apparent diffusivity *KD* of the peptides in the network during release. Table 2 shows that *KD* values are at least one or two orders of magnitude smaller than the diffusivities in water (Table 1). The result and its interpretation will be discussed in detail later. Note, however, that the model takes into account that the microgels swell during release in such a way that, in principle, *KD* should be constant. The fact that *KD* is lower than D_0 shows that the peptides were immobilised inside the microgel. The different *KD* values observed for the peptides reveal differences in their interaction pattern inside the microgels.

3.2. SCISSOR results

Fig. 8 shows the result from the SCISSOR experiments as plots of fraction released *vs*. time. The fraction released is defined as the amount transported to the release medium outside the cartridge divided by the amount of peptide injected into the cartridge. Because the stability of the SCISSOR matrix is guaranteed for only 24 h, we will only include the initial part of the release curves in the kinetic analysis. However, we show the long-time behaviour for reference. We quantified the release rate by determining the release rate constant *k*, defined as the slope of the initial (semi-) linear part of the release profiles, see Eq. (4). We also calculated the ratio k/D_0, where D_0 is the peptide's diffusion coefficient in water. A small value of k/D_0 indicates that the net mass transfer from the depot to the release medium is affected comparatively much by interactions with the extracellular matrix-mimicking components inside the cartridge (see Materials and methods). One release experiment was conducted for each peptide.

3.2.1. Exenatide

The peptide was injected as a 40 mg solution in 0.5 ml DI water. During the first 24 h, ca. 70 % of the peptide was released at a fairly constant rate. The recorded light transmission revealed a 10–20 % lowering of the transmittance during that period. At longer times, a plateau was reached after ca. 80 % had been released. After 48 h, the release suddenly increased again, and when the experiment was stopped after 52 h, 90 % had been released. From the initial part of the release curve we obtained the release rate constant $k = 0.029\ h^{-1}$, and $k/D_0 = 4.8\ cm^{-2}$. The orders of magnitude are those expected for the release from a solution depot and free diffusion of the peptide out of the

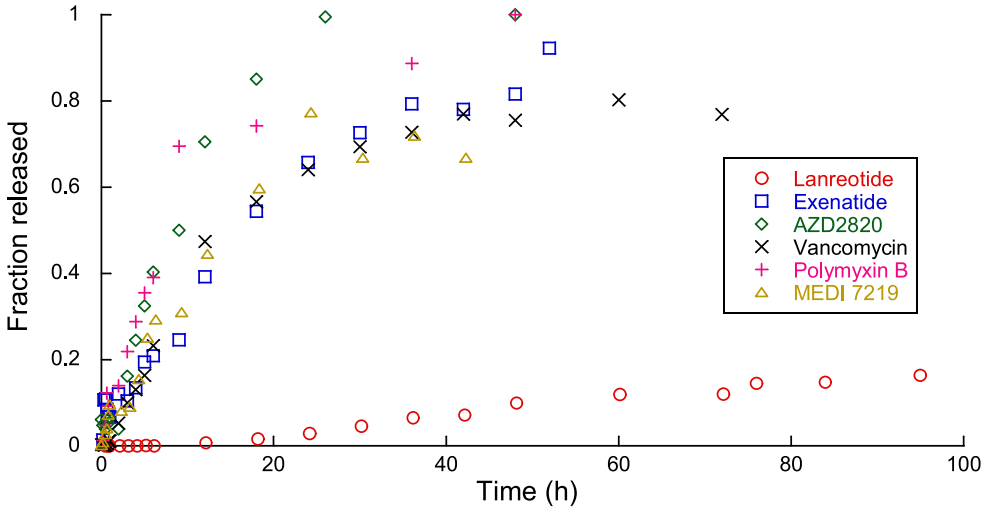

Fig. 8. Release profiles recorded with SCISSOR showing the fraction released *vs*. time after injection of the formulation into the cartridge containing the HA solution. The fraction released is the fraction transferred from the cartridge to the compartment containing the carbonate buffered release medium (pH 7.4). One release experiment for each peptide was conducted (n = 1) Temperature: 34 °C.

cartridge (see above), suggesting that most of the injected peptide molecules remained solubilised in the depot, with only a minor part "immobilised" by aggregation or precipitation. Considering the negative charge of the peptide, the interpretation is in agreement with expectations.

3.2.2. Vancomycin

The peptide was injected as a 60 mg/ml aqueous solution. The shape of the release profile with final fractional release of ca. 80 %, was that expected for a first-order release (Eq. S:17) from a solution depot with a fraction of immobilised peptide. From the model fit of the release profile we obtained $k = 0.040\ h^{-1}$ showing that the fractional release increased faster than for exenatide. However, since $k/D_0 = 3.6\ cm^{-2}$ is smaller than for exenatide, the difference can be attributed mainly to vancomycin's higher intrinsic diffusivity in water (lower molecular weight).

3.2.3. Polymyxin B

The peptide was injected as a 100 mg/ml aqueous solution. The shape of the release profile resembles that of vancomycin but complete release was obtained after ca. 48 h, which is larger than 24 h for which SCISSOR is validated. No lowering of light transmittance was recorded, indicating the absence of detectable aggregates. The model fit gave $k = 0.076\ h^{-1}$ and $k/D_0 = 5.9\ cm^{-2}$ indicating that the release was rate controlled by diffusive mass transport of the peptide through the HA solution.

3.2.4. Pramlintide

The peptide was injected as a turbid, 75 mg/ml pramlintide suspension in water (Fig. S16), and remained as an aggregated bolus inside the cartridge during the entire experiment. No pramlintide was detected in the release medium during the time of the experiment (72 h). Concentrations closer to the ones used in the clinic (1 mg/ml, 30–120 μg) were not investigated because of the limitations of the spectroscopy method used for detection.

3.2.5. Lanreotide

The peptide was prepared as a 50 mg/ml aquesous solution. After injection, the solution immediately formed a turbid bolus in the HA-matrix (Fig. S16), and the light transmittance in the cartridge was lowered by 90 %. The release profile revealed slow and incomplete release, with the released fraction reaching only 40 % even after 95 h. The incomplete release was evident also from the substantial amounts of aggregated peptide remaining after the experiment was finished (Fig. S16). The model fit gave $k = 0.0024\ h^{-1}$ and $k/D_0 = 0.18\ cm^{-2}$ indicating that a large fraction of the peptide was immobilized by aggregation, and formed a sustain-release depot embedded in the HA matrix.

3.2.6. AZD2820

The peptide, injected as a 60 mg/ml aqueous solution, resulted in no detectable aggregation. The release profile has the shape expected for a first-order process involving a droplet of a peptide solution and diffusive mass transport through the HA-matrix. The model fit gave $k = 0.10\ h^{-1}$ and $k/D_0 = 7.3\ cm^{-2}$, and the fraction released reached 100 % after 30 h. The result suggests that the process was rate controlled by the diffusion of the peptide out of the cartridge, without appreciable effects from interaction with the matrix components.

3.2.7. MEDI7219

The peptide was injected as a 132 mg/ml aqueous solution. The major part was rapidly released, but the fraction released levelled off at ca. 80 %. The injection caused a lowering of the transmittance by 10–20 %, suggesting that the incomplete release was due to irreversible aggregation of a fraction of the peptide. The model fit gave $k = 0.036\ h^{-1}$ and $k/D_0 = 3.1\ cm^{-2}$. Taken together, the behaviour resembled that of vancomycin.

3.3. Relationships between MIS parameters

The thermodynamic parameters provided by MIS are CCC, C_{pep}^{liq}, C_{pep}^{gel} and V_∞/V_{150}. The first two describe the peptide concentration in the solution in equilibrium with fully loaded microgels. They coincide for systems displaying a VPT and will be used as measures of the stability of peptide-HA complexes and/or the strength of interaction between peptide and HA. C_{pep}^{gel} is the peptide concentration in the microgel in the most contracted state after peptide loading and V_∞/V_{150} is the fractional volume recovery of the microgels at the end of the release experiment; both will be used as measures of the peptide aggregation tendency. CCC, C_{pep}^{liq} and V_∞/V_{150} are read directly from the experimental curves and are therefore model independent parameters. In contrast, the parameters *aD* and *KD*, describing transport properties, are model dependent (see above). Below we will put much emphasis on *KD*. To be clear about what the product expresses, we recollect that the swelling rate in the model is controlled by the rate of peptide diffusive mass transport to the microgel surface from a core of peptide-HA complexes. It means that, at every instance during release, the swelling ratio is determined by the amount of peptide remaining in the core. *K* is a partition coefficient equal to the ratio of the concentration of "dissolved" peptide in the internal depletion layer in direct contact with the core and the concentration of peptide in the core, and *D* is the peptide's diffusion coefficient in the depletion layer surrounding the core in the microgel. By dividing *KD* with the diffusion coefficient in water D_0 we obtain a quantity that reflects more directly how the interaction with HA affects the release rate. In principle, KD/D_0 should decrease with increasing stability of the peptide-HA complexes. In conflict with that, we found no simple relationship between KD/D_0 and C_{pep}^{liq} (Fig. S18), in spite of the fact that a low peptide concentration in the solution in equilibrium with the microgels should mean high stability, and *vice versa*. However, we explain that by noting that the two quantities were determined at very different ionic strengths. Thus, equilibrium properties were only investigated at low ionic strength where the thermodynamic driving force for binding is dominated by counter ion entropy. In contrast, at the high ionic strength of the release medium, the entropic effect is largely absent, and other electrostatic effects dominate.

Fig. 9A shows the relationship between KD/D_0 and the net charge Z of the peptide in the release medium. The plot shows that electrostatic attraction plays a role but it is clear that the peptides cannot be ranked with respect to the apparent diffusivity based on charge number only. This underscores the importance of other types of interaction, e.g., hydrophobic interaction between peptides, favouring their self-assembly or aggregation. Previous studies of protein and peptide binding to polyelectrolyte microgels show that aggregation may lead to rigid, porous structures inside microgels hindering contraction of the polymer network (Andersson and Hansson, 2018). The parameter C_{pep}^{gel} has the capacity to report about that type of aggregation because it describes the peptide concentration in the fully loaded microgel.

Fig. 9B shows that there is a rather strong relationship between C_{pep}^{gel} and KD/D_0 involving all peptides except vancomycin. At low ionic strength, all peptides with charge number + 2 or larger will be enriched inside the microgels because of the strong entropic driving force from replacing monovalent counterions to the network with multivalent species. The enrichment will increase the probability of aggregation, and "sticky" peptides interacting with hydrophobic attractions can rapidly start to build up random, porous networks (i.e., small C_{pep}^{gel}). Once formed, hydrophobically stabilized aggregates will be little affected by variations in the ionic strength. As a result, aggregation will reduce the apparent diffusivity measured during release at physiological ionic strength because a fraction of the peptides is immobilised. Within the release model, that means small *K* and therefore small KD/D_0. In contrast, very high packing density requires strong *electrostatic* interactions between the components (Hansson, 2020; Andersson and

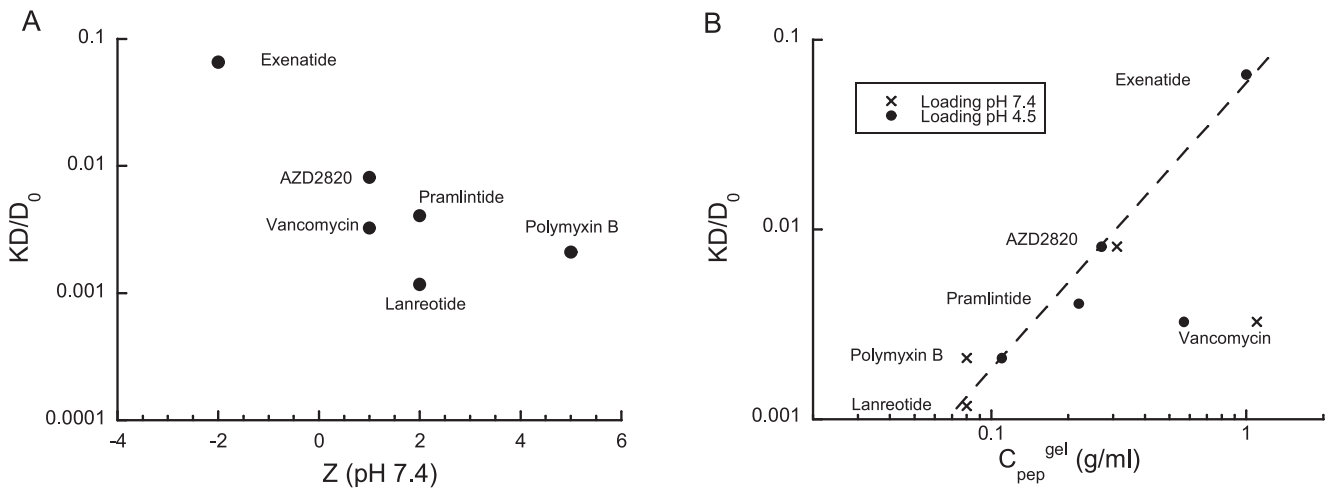

Fig. 9. Relationships between parameters obtained from MIS. **A**: Normalized apparent diffusivity (KD/D_0) plotted *vs.* peptide charge in microgel at pH 7.4. **B**: KD/D_0 plotted *vs.* concentration of peptide in fully loaded microgel (C_{pep}^{gel}) determined after loading at pH 4.5 and 7.4 as indicated. Dashed line is just a guide to the eye.

Hansson, 2017), often referred to as polyelectrolyte-mediated attractions (Forsman, 2006) (ion-ion correlation and polyion-bridging (Podgornik et al., 1995; Åkesson et al., 1989)). The interactions are screened by salt but increase in magnitude with increasing charge density, and are therefore particularly important for multivalent species or highly charged self-assemblies at low ionic strength. Hence, under loading conditions they promote the formation of dense peptide-HA complexes (large C_{pep}^{gel}), but in the release medium they are much weaker because of the high ionic strength, and so their tendency to stabilise peptide-HA complexes and hinder the release of the peptide from the microgel is small (large KD/D_0). We conclude that a gradual crossover from peptides forming porous aggregates, stabilized by hydrophobic interactions, to dense complexes stabilised by electrostatic interactions largely explains the trend observed in Fig. 9B. Lanreotide and pramlintide fit nicely into this picture since they are known to form hydrophobically stabilised aggregates/self-assemblies in aqueous solutions (Pouget et al., 2010; Cort et al., 2009; Brunzell et al., 2024; Pieri et al., 2022). The volume recovery of microgels was low for both peptides (Table 2), suggesting a large fraction of immobilized, perhaps irreversibly aggregated peptide in the microgel. At the same time, the swelling curves (Fig. 7) show that the mobile fraction was quickly released, with implications for the interpretation of the *in vivo* data (see below). For pramlintide another indication of aggregation was that the microgels lost their spherical shape for the higher concentration of 2 mg/ml (Fig. S12). The images also show that aggregates formed in the solution inside the chip at pH 4.5, which remained after changing to the release medium. For polymyxin B, which is not known to form aggregates in aqueous solution, we attribute its position in Fig. 9B to its high positive charge. Thus, the small KD/D_0-value is explained by a small diffusion coefficient in the HA network because of strong coulomb attraction to the HA network even in monomeric form; the low C_{pep}^{gel} is explained by the peptide binding as monomer rather than forming highly charged micelles. This explanation is in accord with the extended release time and the high microgel volume recovery (Fig. 6) indicating that the interactions are dominated by electrostatic forces. We speculate that the initial "fast" swelling (Fig. 7) was caused by the rapid release of a portion of the peptide bound to the microgels in excess of that required for charge stoichiometry. AZD2820's apparent diffusivity was two orders of magnitude smaller than the diffusion coefficient in water. Since the peptide is expected to be monovalent at pH 7.4 its position in Fig. 9B suggests that it formed small self-assemblies in local equilibrium with monomers. Previous works show that charged micelles with small aggregation numbers can induce a fairly large collapse without giving rise to a VPT, in agreement with the results from the loading experiment. Exenatide, which is positively charged inside the microgels in the loading medium at pH 4.5, displayed a VPT, suggesting that it self-assembled inside the microgel. The large C_{pep}^{gel}-value is explained by the formation of micelles interacting with HA with strong electrostatic forces giving rise to dense complexes. However, since it becomes negatively charged (−2) in the release medium at pH 7.4, D is expected to deviate little from D_0. Therefore, the fact that $KD < D_0$ is explained by the local stability of the peptide-HA complexes in the core of the microgel (i.e. $K < 1$). This is in agreement with previous results showing that microgels with a dense core of micelle-polyion complexes can be thermodynamically stable even with 0.15 M NaCl present in the solution (Al-Tikriti and Hansson, 2020; Al-Tikriti and Hansson, 2022). Vancomycin's deviating behaviour may represent a third type of mechanism in which the peptide forms closed self-assemblies stabilised by hydrophobic peptide-peptide interactions rather than porous networks, and that the electrostatic interactions mediated by HA bring those "primary" complexes together into very dense structures. A similar mechanism has been proposed for the interaction between lysozyme and polyelectrolytes (Andersson and Hansson, 2018; Cousin et al., 2010; Cousin et al., 2005; Gummel et al., 2006).

3.4. Relationships between MIS and SCISSOR parameters

The release rate constant k obtained from SCISSOR normalised by the peptide's diffusion coefficient in water D_0 provides information about how the release is affected by interactions with HA. We found no simple relationships between k/D_0 from SCISSOR and C_{pep}^{gel} or KD/D_0 from MIS. However, Fig. 10 shows k/D_0 plotted *vs.* C_{pep}^{liq} obtained from the MIS loading experiments at pH 7.4. The result shows that the stronger the peptide interacted with HA in MIS, the more was the peptide's release affected by the interaction with HA in SCISSOR. While the result as such is in agreement with expectations, it is not completely obvious considering the poor correlation between C_{pep}^{liq} and KD/D_0 (Fig. S18). However, it illustrates that a number of different properties may influence the outcome for the investigated set of peptides.

3.5. Comparison between MIS and SCISSOR parameters and in vivo endpoints

Table 3 shows pharmacokinetic (PK) parameters available for exenatide, AZD2820, pramlintide and lanreotide derived from absorption studies after SC injection in humans. For the other peptides in this work no human data were available. The time to highest peptide plasma

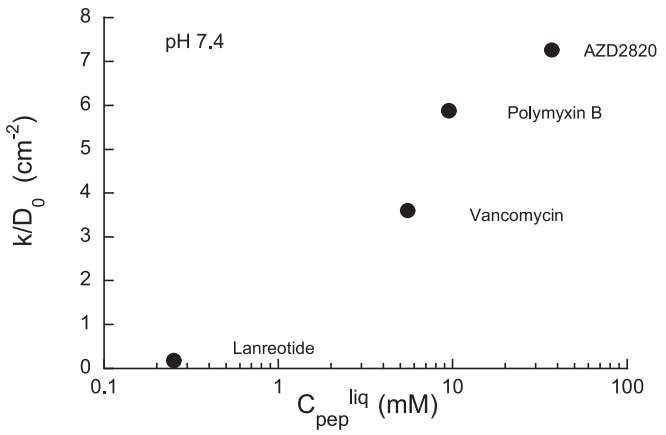

Fig. 10. SCISSOR release rate constant (k) normalized by peptide diffusion coefficient in water (D_0) plotted *vs*. peptide concentration in the liquid in equilibrium with microgel (C_{pep}^{liq}) from MIS (PB; pH 7.4).

Table 3
Human *in vivo* endpoints. Time to highest peptide concentration in blood (t_{max}), peptide half-life ($t_{1/2}$), elimination rate constant (k_e), absorption rate constant (k_a), and bioavailable fraction (F), gathered from literature or received from AstraZeneca, Gothenburg.

Peptide (dose)	$\mathbf{t_{max}}$ (h)	$\mathbf{t_{1/2}}$ (h)	$\boldsymbol{k_e}$ (h^{-1})	$\boldsymbol{k_a}$ (h^{-1})	**F (%)**
Exenatide[a] IRF (≤ 10 μg)	1.5–3	1.5–4	0.55	0.5	51-62[b]
AZD2820[c]	1	2.5-4[d]	0.2–0.3	2–3	N/A
Pramlintide[e]	0.33	0.75–1	0.8	8	30–40
Lanreotide[f]					
IRF (7 μg/kg)	0.25	1.7	0.43	14	70-100[g]
Autogel (60 mg)	9	5-9x10[2]		0.002	60-83[h]

a) Data from (Kolterman et al., 1996; Linnebjerg et al., 2007; Calara et al., 2005; Kolterman et al., 2005; Gao and Jusko, 2011; Gedulin et al., 2008).
b) Value is calculated from a study in rat (Gao and Jusko, 2011; Gedulin et al., 2008) human bioavailability data was not found in literature.
c) AstraZeneca data on file. Animal studies were performed at an Association for Assessment and Accreditation of Laboratory Animal Care (AAALAC) accredited facility with humane care, and all protocols and procedures were approved by the respective country and institutional animal care committees.
d) Dose dependent.
e) Data from (Kellmeyer et al., 2007; Kolterman et al., 1996; Singh-Franco et al., 2007).
f) Data from (Antonijoan et al., 2004; Trocóniz et al., 2009).
g) Estimated based on the relative bioavailability of 82 % between 7 μg/kg and 60 mg dose and F values for 60 mg.
h) Data from Ipsen Bipharmaceuticals: Somatuline package insert (2014); Product Monograph including patient medication information, Somatuline Autogel (2006).

concentration (t_{max}), the half-life of peptide ($t_{1/2}$), and the bioavailable fraction (F) are from direct measurements; the apparent 1st order rate constants for absorption (k_a) and elimination (k_e), respectively, are model dependent. The k_e values for lanreotide are based on experimentally established 1st order kinetics and given as reported in (Antonijoan et al., 2004). For exenatide, k_e was calculated from the parameters determined in (Cirincione and Mager, 2017), which for the therapeutically relevant doses of the immediate release formulation (IRF) are consistent with a linear elimination process and 1st order kinetics, as concluded by the authors of that paper. For AZD2820 and pramlintide, the k_e values were calculated from $t_{1/2}$ assuming 1st order kinetics (k_e=(ln2)/$t_{1/2}$), which for pramlintide is supported by the plasma concentration profiles (Kellmeyer et al., 2007; Kolterman et al., 1996) and the dose independence of $t_{1/2}$ (Singh-Franco et al., 2007). For AZD2820, pramlintide and the IRF of lanreotide, the k_a values are apparent 1st order absorption rate constants calculated from t_{max} and k_e using the relationship valid for a 1-compartment model (Garrett, 1994):

$$t_{max} = \frac{\ln(k_a/k_e)}{k_a - k_e} \tag{5}$$

Antonijoan et al. (Antonijoan et al., 2004) showed that the decay rate of the plasma concentration, following an initial burst release, was very slow for the prolonged-release lanreotide (Autogel) formulation, and suggested that it was dominated by the absorption rate (flip-flop kinetics). The k_a value for Autogel in Table 3 is the decay rate at long times reported by these authors. The value is in close agreement with the long-time absorption rate constant (0.001 h^{-1}) obtained from a model by Troconiz et al. (Trocóniz et al., 2009) involving a time dependent k_a. For exenatide, Cirincione and Mager (Cirincione and Mager, 2017) have modelled the absorption as a sequential process with zero-order kinetics followed by a saturable nonlinear process. However, for low doses (5 and 10 μg) they concluded that the relevance of the nonlinear absorption was minimal. The k_a value for exenatide in Table 3 was obtained from a 1-compartment model with 1st order absorption and elimination kinetics providing a good fit to human *in vivo* data (Fig. S19). The value is in good agreement with the apparent 1st order rate constant (0.4 – 0.5 h^{-1}) obtained with the nonlinear model in (Cirincione and Mager, 2017) for the major part of the absorption process.

Below we focus on the absorption rate constant, which is the relevant parameter for comparison with the MIS and SCISSOR results. Table 3 shows that k_a for the peptide formulations follows the order lanreotide (Autogel) < exenatide < AZD2820 < pramlintide < lanreotide (IRF). The large difference in k_a between the two lanreotide formulations is explained by the fact that Autogel aggregates *in vivo* (Trocóniz et al., 2009) while IRF does not.

3.5.1. SCISSOR

Fig. 11A shows k_a plotted *vs*. the rate constant k determined with SCISSOR. Because no data were obtained for pramlintide the data set is limited, but the plot suggests that the predictive capacity of the method is good also for small peptide drugs, earlier shown to be the case for large biologics (Bown et al., 2018; Torres-Terán et al., 2023). Aggregation of lanreotide (Autogel) after injection both in the SCISSOR setup and in humans explains why k and k_a are lower than for the other peptides. However, the difference between exenatide and AZD2820 is much larger than expected from the difference in intrinsic diffusivity (D_0). By excluding lanreotide (Autogel), the data in Table 3 suggest that k_a for the other peptide formulations depends on their charge at pH 7.4. A possible explanation is that the charge controls the peptides' tendency to be transferred from the formulation to the ECM. Thus, the negatively charged exenatide (−2) is expected to be partly excluded from the ECM due to the presence of negatively charged hyaluronate and chondroitin sulfate in ECM. In contrast, the transfer of the positively charged peptides is expected to be favoured by the electrostatics, and more so with increasing charge number (within certain limits; see below). We now assume that the absorption rate is governed by pseudo-steady state diffusion through the ECM from a spherical liquid depot of volume V and area A, to blood capillaries located an average distance L from the depot. Then, by Fick's 1st law, $k_a = ADK/LV = 3DK/rL$, where r is the radius of the depot and $K = C_{ECM}/C_{depot}$ is a partition coefficient describing the peptide's partition between ECM and the depot. In case of a difference in average electrostatic potential $\Delta\varnothing$ between the ECM and the depot due to the presence of charged biopolymers in ECM, $K = exp\{-Ze\Delta\varnothing/kT\}$ when considering only electrostatic contributions to K. Fig. 11B shows plots of k_a determined *in vivo vs*. k_a calculated from the relationship $k_a = 3D_0 exp\{-Ze\Delta\varnothing/kT\}/rL$. The plots are valid for $r = 5$ mm and $L = 200$ μm, for which the numbers are realistic but arbitrarily chosen. The result shows that the model describes quite well the peptides' rank order with respect to k_a. Moreover, with $e\Delta\varnothing/kT = -0.5$ the calculated values are of correct order of magnitude. In the latter case, K is 0.37, 1.6, 2.7, and

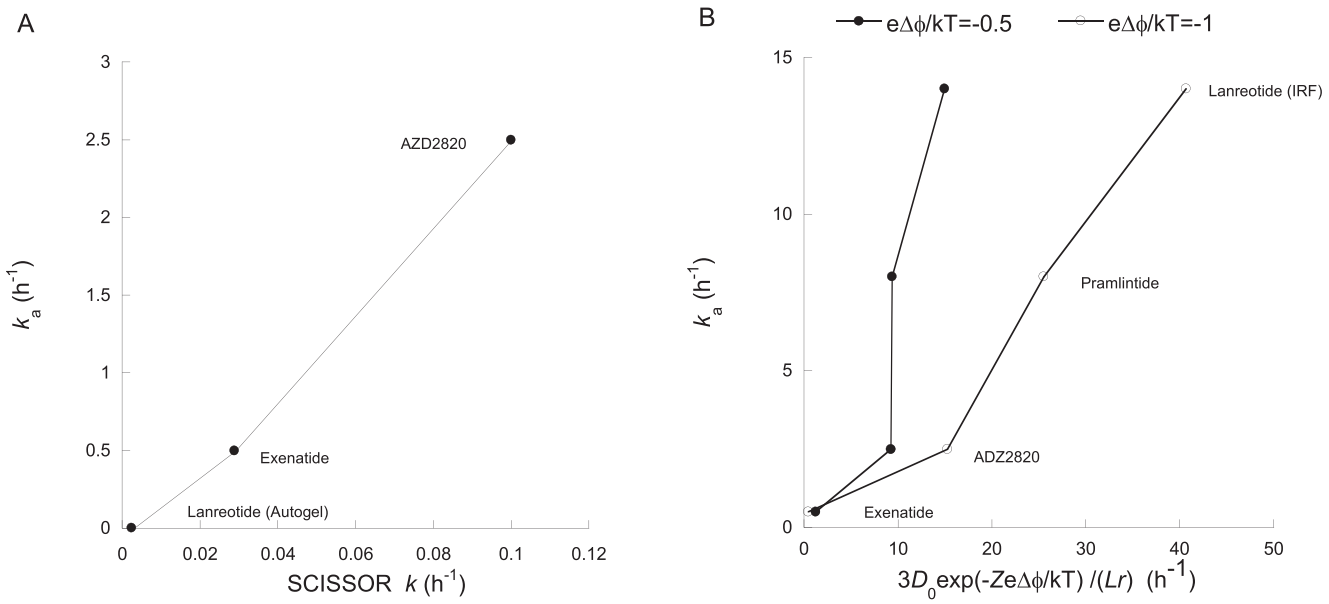

Fig. 11. Apparent 1st order absorption rate constant (k_a) after subcutaneous administration in humans plotted *vs.* (**A**) the release rate constant k determined with SCISSOR, and (**B**) theoretically calculated absorption rate constant calculated from the peptides' diffusivity in water (D_0) and charge number (Z) for two different reduced electrostatic potential differences between depot and ECM as indicated; $r = 5$ mm and $L = 200$ μm (see *3.5.1*). k_a values taken from Table 3.

2.7 for exenatide, AZD2820, pramlintide and lanreotide, respectively. The values are realistic for the partitioning between a depot and ECM, in particular when local environment in is influenced by the low ionic strength of the formulation. From a general point of view, it is interesting that k_a for the negatively charged exenatide is much smaller than for the positively charged peptides, because earlier studies have shown that the transport of positively charged species through the ECM is more hindered than negatively charged species (Richter et al., 2012; Richter and Jacobsen, 2014; Reed et al., 1989; Wiig and Swartz, 2012). Those results are based mainly on studies of large proteins and nanoparticles, typically carrying many charges. Clearly the diffusivity of highly charged cationic peptides like polymyxin B (+5) are expected to be reduced by electrostatic interactions with negatively charged polysaccharides, as was recently demonstrated for polylysine in a hydrogel model of the extracellular matrix (Parlow et al., 2024). However, for peptides carrying one or two positive charges, the effect will be small at physiological ionic strength, and k_a is expected to be dominated by the partition coefficient between the depot and ECM, which is not directly related to the diffusivity in ECM. Of course, we do not exclude other explanation as for the relationship between peptide charge and k_a. For example, the negatively charged glycosaminoglycans in the glycocalyx layer of the blood vessel epithelium, known to affect the exchange of molecules between the blood and tissues (Adamson et al., 1988) (Stace and Damiano, 2001), may give rise to a similar dependency on peptide charge as the one depicted here. Peptide binding to albumin may be another contributing factor, since negatively and positively charged species are known to interact differently with albumin (Gallo et al., 2022) (Rahimizadeh et al., 2020). However, the fact that exenatide (Śliwińska-Hill and Wiglusz, 2020) and lanreotide (Barbanoj et al., 1999) but not pramlintide (Singh-Franco et al., 2007) have been reported to bind extensively to albumin, speaks against a dominating influence of albumin on the observed k_a-ranking order of the peptides. Another factor that may affect the pharmacokinetics of the peptides in different ways, not considered here, is of course catabolic degradation (Varkhede et al., 2020; Esposito et al., 2020).

3.5.2. MIS

We have found no physically comprehensible relations between k_a and the parameters KD and C_{pep}^{gel}. Nevertheless, below we show that MIS-derived parameters have the capacity to predict important *in vivo* properties of the peptides.

As indicated above, the plasma profile for Autogel is characterised by a minor burst release (Antonijoan et al., 2004; Trocóniz et al., 2009), showing that a small, freely mobile fraction is rapidly absorbed. This is in agreement with the high k_a value for the IRF, showing that freely mobile lanreotide is rapidly absorbed. The slow 1st order absorption process for Autogel requires the mobile fraction in the depot to decrease relative to the total amount in the depot. This can be accomplished if the dissolution rate is a function of the aggregate area exposed to the liquid, which is expected to decrease with decreasing amount of aggregated peptide. By assuming that the mobile fraction has the same diffusivity as in the IRF, the mobile fraction in the Autogel depot should be roughly equal to $k_a(\text{Autogel})/k_a(\text{IRF}) = 0.002/14 \approx 1.4 \times 10^{-4}$. The corresponding estimate from the apparent diffusivity KD is obtained by assuming that D and D_0 are of the same order of magnitude, so that $K \approx KD/D_0 \approx 8.8 \times 10^{-4}$. Thus, MIS is able to account for the fact that the apparent 1st order absorption rate constant for Autogel is more than 10^3 times smaller than for the IRF.

KD is a measure of the apparent diffusivity of a peptide through the HA network in the microgels. In principle, it should be related to the diffusivity in the ECM, and hence to k_a if the transport rate through ECM is controlling the absorption rate. In contrast, when lanreotide (Autogel) is excluded from the comparison, KD increases when k_a decreases (Fig. S20). We have found no meaningful way to explain that relationship. However, the result does not imply that the MIS results are in conflict with the *in vivo* data. As pointed out above, the variation in KD for the present set of peptides is dominated by K, describing the local partitioning of the peptide between complexes/aggregates in the core of the microgel and the swollen HA network in the shell. Because of that, it is primarily related to the stability and dissolution rate of the complexes/aggregates, as indicated by the order of the peptides when ranked by increasing value of KD: lanreotide < pramlintide < AZD2820 < exenatide. The same order is obtained when ranked by increasing value of the other indicator of aggregation C_{pep}^{gel} (Fig. S20). How can we explain that the reverse order is obtained when the peptide formulations, including both lanreotide (IRF) and (Autogel), are ranked in order of increasing value of k_a? As already shown, the very low KD, indicative of low dissolution rate of the aggregates, explains the position of

lanreotide (Autogel) in the list. Pramlintide formulations precipitate at pH > 5.5 (Singh-Franco et al., 2007), and the peptide has been shown to rapidly form amyloid fibrils at pH 7.4 in 50 mM phosphate buffer (although much slower in 50 mM Tris buffer) (da Silva et al., 2016). Considering the low bioavailability (30–40 %) yet very high k_a, it is likely that the depot contains one fraction that is freely mobile and one fraction that is irreversibly precipitated/aggregated. This is also in agreement with the MIS results (see above). Thus, we believe that the order of exenatide, AZD2820, pramlintide and lanreotide (IRF) is chiefly explained by the partitioning of solubilized peptide between the depot and ECM determined by their charge. In contrast, the ranking order with respect to *KD* reflects how the release rate depended on the dissolution rate of peptide-HA complexes formed in the microgel during loading at low ionic strength.

The results from the MIS binding study at pH 7.4 (Figs. 3 and 5) show that exenatide did not enter the microgels, and that AZD2820 and lanreotide both entered but the concentration required to induce a volume change was clearly lower for lanreotide than AZD2820. (For pramlintide, no data was obtained at pH 7.4). Since the inverse of the peptide concentration in the solution in equilibrium with the microgels can be interpreted as a conditional binding constant, the order of the peptides when ranked by increasing binding strength becomes exenatide < AZD2820 < lanreotide. This is the same order as when ranked after increasing k_a (exenatide < AZD2820 < lanreotide (IRF)). Because strong binding to HA microgels should, in general, favour the partitioning from solutions to HA-rich environments, the relationship between increased binding strength to HA and increasing k_a is in agreement with the above hypothesis that k_a increases with increasing partition coefficient between depot and ECM. This also explains the relationship between k/D_0 (SCISSOR) and C_{pep}^{liq} (MIS) in Fig. 10A.

4. Conclusions

Our results show that the MIS method can provide qualitative and quantitative information about the interaction strength between pharmaceutical peptides and hyaluronic acid, as well as the peptides' diffusivity and aggregation behaviour in HA networks. It is possible to distinguish between two types of idealized behaviour. In one extreme end are peptides forming micelle-like self-assemblies in complexes with HA. In the microgel, at low ionic strength, individual self-assemblies are held together by strong coulomb attractions mediated by the oppositely charged network chains. As a result, the peptide concentration in the microgel C_{pep}^{gel} is very high. At physiologically relevant ionic strengths the complexes gradually dissolve because the interaction with HA is weakened in the presence of salt. Of the same reason, the dissolved peptides rapidly diffuse out of the microgel under sink conditions, resulting in high apparent diffusivity *KD*. In the other extreme are 'sticky' peptides forming aggregates stabilised by non-electrostatic (hydrophobic) forces. When loaded onto microgels they form (random) porous aggregates, and so C_{pep}^{gel} is comparatively low. Because hydrophobic interactions are insensitive to salt, the aggregated fraction is effectively immobilised even under physiological conditions, resulting in low *KD*. For the majority of the investigated peptides, a high C_{pep}^{gel} corresponds to high *KD* and *vice versa*. They can be ranked by increasing value of either C_{pep}^{gel} or *KD*: lanreotide < polymyxin B < pramlintide < AZD2820 < exenatide; the reversed order means increasing tendency to aggregate in complexes with HA. Vancomycin deviates from the pattern by having high C_{pep}^{gel} and low *KD* and may represent a third type of behaviour in which peptide aggregates are stabilised by hydrophobic forces without being sticky. When used to classify the peptides as aggregating or non-aggregating, MIS and SCISSOR gave similar results.

Based on a small data set including lanreotide (Autogel), exenatide and AZD2820, the SCISSOR release rate constant k appears to correlate with the apparent 1st order absorption rate constant k_a derived from SC administrations in humans, suggesting that the method's predictive capacity, previously demonstrated for antibodies, may extend to small peptides. In contrast, no such correlation between the MIS parameters and k_a could be established. However, the minimum concentration of peptide in the solution required to detect a microgel volume change in MIS binding studies (or alternatively C_{pep}^{liq}) can be used to predict the order of the peptides when ranked by increasing k_a. The order is the same as when the peptides are ranked after increasing positive charge, suggesting that the absorption rate constant increases with increasing partitioning from the formulation to the ECM. Furthermore, MIS is able to account for the burst release observed after SC injection of lanreotide (Autogel), i.e., that a non-aggregated fraction is rapidly released, and for the fact the apparent 1st order absorption rate constant for Autogel is more than 10^3 times smaller than for the IRF. In general, comparison between MIS and SCISSOR shows that the methods provide complementary information partly in agreement with each other.

In future work, apart from evaluating the predictive capacity of MIS for other sets of peptide and protein drugs, the capacity of the method to capture more effects can be extended by employing microgels of other extracellular matrix polyelectrolytes, such as chondroitin sulfate and heparan sulfate, and including other tissue specific macromolecules, such as albumin and fibronectin, in the liquid medium. Desirable future technical improvements include the possibility to monitor the distribution of molecules inside the microgels, e.g. by fluorescence microscopy, or to determine the bound amount. It is a strength of the present method that interactions can be probed simply by monitoring microgel volume changes. However, direct measurement of the bound/released amount would, e.g., avoid the difficulty of discriminating between incomplete release and irreversible or very slow changes of the microgel network structure, a problem encountered in this work and elsewhere (Wanselius et al., 2022; Wanselius et al., 2023).

The present work shows that MIS provides physicochemical data that can be used to predict specific aspects of peptide drug absorption *in vivo*. However, rather than being used as a stand-alone technique, the great merit would come from using the results together with complementary results from other methods in combination with (*in silico*) physiologically based biopharmaceutics modelling. Other relevant methods under development in our lab are fluorescence-recovery after photo bleaching (FRAP) providing self-diffusion coefficients, and measurements of diffusive mass transfer in models of the extracellular matrix.

CRediT authorship contribution statement

Marcus Wanselius: Writing – original draft, Visualization, Validation, Methodology, Investigation, Formal analysis, Data curation, Conceptualization. **Susanna Abrahmsén-Alami:** Writing – review & editing, Supervision, Resources, Funding acquisition, Conceptualization. **Belal I. Hanafy:** Writing – review & editing, Validation, Methodology. **Mariarosa Mazza:** Writing – review & editing, Validation, Methodology. **Per Hansson:** Writing – review & editing, Writing – original draft, Validation, Supervision, Project administration, Methodology, Investigation, Funding acquisition, Formal analysis, Data curation, Conceptualization.

Declaration of competing interest

The authors declare that they have no known competing financial interests or personal relationships that could have appeared to influence the work reported in this paper.

Acknowledgments

This study is part of the science program of the Swedish Drug Delivery Center (SweDeliver) and financial support from Vinnova (Dnr 2019-00048) is gratefully acknowledged. The SCISSOR experiments

were performed at AstraZeneca, Cambridge, while parts of the *in vivo* data used were acquired from AstraZeneca, Gothenburg.

We thank Carl-Gustav Sigfridsson for support regarding the properties and *in vivo* behavior of pramlintide.

Appendix A. Supplementary data

Supplementary data to this article can be found online at https://doi.org/10.1016/j.ijpharm.2024.124849.

Data availability

Data will be made available on request.

References

Adamson, R.H., Huxley, V.H., Curry, F.E., 1988. Single capillary permeability to proteins having similar size but different charge. Am. J. Phys. Anthropol. 254 (2 Pt 2), H304–H312.

Ahnfelt, E., Gernandt, J., Al-Tikriti, Y., Sjögren, E., Lennernäs, H., Hansson, P., 2018. Single bead investigation of a clinical drug delivery system – A novel release mechanism. J. Control. Release 292, 235–247.

Åkesson, T., Woodward, C., Jönsson, B., 1989. Electric double layer forces in the presence of polyelectrolytes. J. Chem. Phys. 91, 2461–2469.

Al-Tikriti, Y., Hansson, P., 2020. Drug-Eluting Polyacrylate Microgels: Loading and Release of Amitriptyline. J. Phys. Chem. B 124 (11), 2289–2304.

Al-Tikriti, Y., Hansson, P., 2022. Drug-Induced Phase Separation in Polyelectrolyte Microgels. Gels 8 (1), 4.

Andersson, M., Hansson, P., 2017. Phase Behavior of Salt-Free Polyelectrolyte Gel-Surfactant Systems. J. Phys. Chem. B 121 (24), 6064–6080.

Andersson, M., Hansson, P., 2018. Binding of Lysozyme to Spherical Poly (styrenesulfonate) Gels, Gels (Basel. Switzerland) 4 (1), 9.

Andersson, M., Råsmark, P.J., Elvingson, C., Hansson, P., 2005. Single microgel particle studies demonstrate the influence of hydrophobic interactions between charged micelles and oppositely charged polyions. Langmuir 21, 3773–3781.

Antonijoan, R.M., Barbanoj, M.J., Cordero, J.A., Peraire, C., Obach, R., Vallès, J., Chérif-Cheikh, R., Torres, M.L., Bismuth, F., Montes, M., 2004. Pharmacokinetics of a new Autogel formulation of the somatostatin analogue lanreotide after a single subcutaneous dose in healthy volunteers. J. Pharm. Pharmacol. 56 (4), 471–476.

Barbanoj, M., Antonijoan, R., Morte, A., Grinyó, J.M., Solà, R., Vallès, J., Peraire, C., Cordero, J.A., Muñoz, A., Jané, F., Obach, R., 1999. Pharmacokinetics of the somatostatin analog lanreotide in patients with severe chronic renal insufficiency. Clin. Pharmacol. Ther. 66 (5), 485–491.

Bender, C., Eichling, S., Franzen, L., Herzog, V., Ickenstein, L.M., Jere, D., Nonis, L., Schwach, G., Stoll, P., Venczel, M., Zenk, S., 2022. Evaluation of In Vitro Tools to Predict the In Vivo Absorption of Biopharmaceuticals Following Subcutaneous Administration. J. Pharm. Sci. 111 (9), 2514–2524.

Benet, A., Halseth, T., Kang, J., Kim, A., Ackermann, R., Srinivasan, S., Schwendeman, S., Schwendeman, A., 2021. The Effects of pH and Excipients on Exenatide Stability in Solution. Pharmaceutics 13 (8).

Bittner, B., Richter, W., Schmidt, J., 2018. Subcutaneous Administration of Biotherapeutics: An Overview of Current Challenges and Opportunities. BioDrugs : Clin. Immunotherap. Biopharmaceut. Gene Therapy 32 (5), 425–440.

Bock, F., Lin, E., Larsen, C., Jensen, H., Huus, K., Larsen, S.W., Østergaard, J., 2020. Towards in vitro in vivo correlation for modified release subcutaneously administered insulins, European journal of pharmaceutical sciences : official journal of the European Federation for. Pharmaceutical Sciences 145, 105239.

Bown, H.K., Bonn, C., Yohe, S., Yadav, D.B., Patapoff, T.W., Daugherty, A., Mrsny, R.J., 2018. In vitro model for predicting bioavailability of subcutaneously injected monoclonal antibodies. J. Control. Release 273, 13–20.

Brunzell, E., Sigfridsson, K., Gedda, L., Edwards, K., Bergström, L.M., 2024. Investigation of supramolecular structures in various aqueous solutions of an amyloid forming peptide using small-angle X-ray scattering. Soft Matter 20 (10), 2272–2279.

Bysell, H., Schmidtchen, A., Malmsten, M., 2009. Binding and Release of Consensus Peptides by Poly(acrylic acid) Microgels. Biomacromolecules 10 (8), 2162–2168.

Bysell, H., Hansson, P., Malmsten, M., 2010. Effect of charge density on the interaction between cationic peptides and oppositely charged microgels. J. Phys. Chem. B 114, 7207–7215.

Calara, F., Taylor, K., Han, J., Zabala, E., Carr, E.M., Wintle, M., Fineman, M., 2005. A randomized, open-label, crossover study examining the effect of injection site on bioavailability of exenatide (synthetic exendin-4). Clin. Ther. 27 (2), 210–215.

Chiang, P.C., Nagapudi, K., Fan, P.W., Liu, J., 2019. Investigation of Drug Delivery in Rats via Subcutaneous Injection: Case Study of Pharmacokinetic Modeling of Suspension Formulations. J. Pharm. Sci. 108 (1), 109–119.

Cirincione, B., Mager, D.E., 2017. Population pharmacokinetics of exenatide. Br. J. Clin. Pharmacol. 83 (3), 517–526.

D.S. Collins, L.C. Kourtis, N.R. Thyagarajapuram, R. Sirkar, S. kapur, M.W. Harrison, D.J. Bryan, G.B. Jones, J.M. Wright, Optimizing the bioavailability of subcutaneous administered biotherapeutics through mechanochemical drivers, Pharmaceutical research 34 (2017) 2000-2011.

Collins, D.S., Sánchez-Félix, M., Badkar, A.V., Mrsny, R., 2020. Accelerating the development of novel technologies and tools for the subcutaneous delivery of biotherapeutics. J. Control. Release 321, 475–482.

Comely, K., Fleck, N., 2011. Deep penetration and liquid injection into adipose tissue. J. Mech. Mater. Struct. 6 (1–4), 127–140.

Cort, J.R., Liu, Z., Lee, G.M., Huggins, K.N., Janes, S., Prickett, K., Andersen, N.H., 2009. Solution state structures of human pancreatic amylin and pramlintide. Protein Engineering, Design & Selection : PEDS 22 (8), 497–513.

Cousin, F., Gummel, J., Ung, D., Boué, F., 2005. Polyelectrolyte-protein complexes: Structure and conformation of each species revealed by SANS. Langmuir 21, 9675–9688.

Cousin, F., Gummel, J., Clemens, D., Grillo, I., Boué, F., 2010. Multiple scale reorganization of electrostatic complexes of poly(styrenesulfonate) and lysozyme. Langmuir. https://doi.org/10.1021/la904398z.

da Silva, D.C., Fontes, G.N., Erthal, L.C.S., Lima, L.M.T.R., 2016. Amyloidogenesis of the amylin analogue pramlintide. Biophys. Chem. 219, 1–8.

Dunning, C., Lame, M.E., Wrona, M., Haynes, K., 2019. Development of a SPE LC-MS/MS Method Utilizing QuanRecovery Sample Plates with MaxPeak High Performance Surfaces for the Bioanalytical Quantification of Pramlintide from Serum. Waters Corporation. https://www.waters.com/content/dam/waters/en/app-notes/2019/720006527/720006527-it.pdf,.

Eichenbaum, G.M., Kiser, P.F., Dobrynin, A.V., Simon, S.A., Needham, D., 1999. Investigation of the swelling response and loading of ionic microgels with drugs and proteins: The dependence on cross-link density. Macromolecules 32, 4867–4878.

Esposito, S., Vanni, D., Menta, S., Orsatti, L., Monteagudo, E., 2020. Comparison of different protein precipitation and solid-phase extraction protocols for the study of the catabolism of peptide drugs by LC-HRMS. Journal of Peptide Science : an Official Publication of the European Peptide Society 26 (9), e3272.

Fathallah, A.M., Balu-Iyer, S.V., 2015. Anatomical, physiological, and experimental factors affecting the bioavailability of sc-administered large biotherapeutics. J. Pharm. Sci. 104 (2), 301–306.

Forsman, J., 2006. Polyelectrolyte mediated forces between macromolecules. Curr. Opin. Colloid Interface Sci. 11, 290–294.

Gallo, M., Vanni, D., Esposito, S., Alaimo, N., Orvieto, F., Rulli, F., Missineo, A., Caretti, F., Bonelli, F., Veneziano, M., Orsatti, L., Monteagudo, E., 2022. Oligomerization, albumin binding and catabolism of therapeutic peptides in the subcutaneous compartment: An investigation on lipidated GLP-1 analogs. J. Pharm. Biomed. Anal. 210, 114566.

Gao, W., Jusko, W.J., 2011. Pharmacokinetic and pharmacodynamic modeling of exendin-4 in type 2 diabetic Goto-Kakizaki rats. J. Pharmacol. Exp. Ther. 336 (3), 881–890.

Garrett, E.R., 1994. The Bateman function revisited: A critical reevaluation of the quantitative expressions to characterize concentrations in the one compartment body model as a function of time with first-order invasion and first-order elimination. J. Pharmacokinet. Biopharm. 22 (2), 103–128.

Gedulin, B.R., Smith, P.A., Jodka, C.M., Chen, K., Bhavsar, S., Nielsen, L.L., Parkes, D.G., Young, A.A., 2008. Pharmacokinetics and pharmacodynamics of exenatide following alternate routes of administration. Int. J. Pharm. 356 (1–2), 231–238.

Gummel, J., Boué, F., Demé, B., Cousin, F., 2006. Charge stoichiometry inside polyelectrolyte-protein complexes: A direct SANS measurement for the PSSNa-lysozyme system. J. Phys. Chem. B 110, 24837–24846.

Hansson, P., 2020. Volume transition and phase coexistence in polyelectrolyte gels interacting with amphiphiles and proteins. Gels 6, 24.

Hansson, P., Bysell, H., Månsson, R., Malmsten, M., 2012. Peptide-microgel interaction in the strong coupling regime. J. Phys. Chem. B 116, 10964–10975.

Hudson, F.M., Andersen, N.H., 2004. Exenatide: NMR/CD evaluation of the medium dependence of conformation and aggregation state. Pept. Sci. 76 (4), 298–308.

Jensen, S.S., Jensen, H., Møller, E.H., Cornett, C., Siepmann, F., Siepmann, J., Østergaard, J., 2016. In vitro release studies of insulin from lipid implants in solution and in a hydrogel matrix mimicking the subcutis, European journal of pharmaceutical sciences : official journal of the European Federation for. Pharmaceutical Sciences 81, 103–112.

Jidheden, C., Hansson, P., 2016. Single microgels in core-shell equilibrium: A novel method for limited volume studies. J. Phys. Chem. B 120, 10030–10042.

Johansson, C., Hansson, P., Malmsten, M., 2009. Mechanism of lysozyme uptake in poly (acrylic acid) microgels. J. Phys. Chem. B 113, 6183–6193.

Johnson, J.L., Yalkowsky, S.H., 2006. Reformulation of a new vancomycin analog: An example of the importance of buffer species and strength. AAPS PharmSciTech 7 (1), E33–E37.

Kabanov, V.A., Skobeleva, V.B., Rogacheva, V.B., Zezin, A.B., 2004. Sorption of proteins by slightly cross-linked polyelectrolyte hydrogels: Kinetics and mechanism. J. Phys. Chem. B 108, 1485–1490.

Kagan, L., Turner, M.R., Balu-Iyer, S.V., Mager, D.E., 2012. Subcutaneous absorption of monoclonal antibodies: role of dose, site of injection, and injection volume on rituximab pharmacokinetics in rats. Pharm. Res. 29 (2), 490–499.

Karabanova, V.B., Rogacheva, V.B., Zezin, A.B., Kabanov, V.A., 1995. Interaction of cross-linked sodium polyacrylate with proteins, Polymer. Science 37, 1138–1143.

Kellmeyer, T.A., Kesty, N.C., Wang, Y., Frias, J.P., Fineman, M.S., 2007. Pharmacokinetics of an oral drug (acetaminophen) administered at various times relative to subcutaneous injection of pramlintide in subjects with type 2 diabetes. J. Clin. Pharmacol. 47 (7), 798–805.

Khokhlov, A.R., Kramarenko, E.Y., Makhaeva, E.E., Starodubtzev, S.G., 1992. Collapse of polyelectrolyte networks induced by their interaction with oppositely charged surfactants. Macromolecules 25, 4779–4783.

Kinnunen, H.M., Mrsny, R.J., 2014. Improving the outcomes of biopharmaceutical delivery via the subcutaneous route by understanding the chemical, physical and

physiological properties of the subcutaneous injection site. J. Control. Release 182, 22–32.
Kinnunen, H.M., Sharma, V., Contreras-Rojas, L.R., Yu, Y., Alleman, C., Sreedhara, A., Fischer, S., Khawli, L., Yohe, S.T., Bumbaca, D., Patapoff, T.W., Daugherty, A.L., Mrsny, R.J., 2015. A novel in vitro method to model the fate of subcutaneously administered biopharmaceuticals and associated formulation components. J. Control. Release 214, 94–102.
Kolterman, O.G., Schwartz, S., Corder, C., Levy, B., Klaff, L., Peterson, J., Gottlieb, A., 1996. Effect of 14 days' subcutaneous administration of the human amylin analogue, pramlintide (AC137), on an intravenous insulin challenge and response to a standard liquid meal in patients with IDDM. Diabetologia 39 (4), 492–499.
Kolterman, O.G., Kim, D.D., Shen, L., Ruggles, J.A., Nielsen, L.L., Fineman, M.S., Baron, A.D., 2005. Pharmacokinetics, pharmacodynamics, and safety of exenatide in patients with type 2 diabetes mellitus. Am. J. Health Syst. Pharm. 62 (2), 173–181.
Kožák, J., Rabišková, M., Lamprecht, A., 2021. In-vitro drug release testing of parenteral formulations via an agarose gel envelope to closer mimic tissue firmness. Int. J. Pharm. 594, 120142.
Leung, D.H., Kapoor, Y., Alleyne, C., Walsh, E., Leithead, A., Habulihaz, B., Salituro, G. M., Bak, A., Rhodes, T., 2017. Development of a convenient In Vitro gel diffusion model for predicting the In ViVo performance of subcutaneous paranteral formulations of large and small molecules. AAPS PharmSciTech 18 (6), 2203–2213.
Li, Y., de Vries, R., Kleijn, M., Slaghek, T., Timmermans, J., Cohen Stuart, M., Norde, W., 2010. Lysozyme uptake by oxidized starch polymer microgels. Biomacromolecules 11, 1754–1762.
Liang, J., Xiao, X., Chou, T.-M., Libera, M., 2019. Counterion Exchange in Peptide-Complexed Core-Shell Microgels. Langmuir 35 (29), 9521–9528.
Linnebjerg, H., Kothare, P.A., Park, S., Mace, K., Reddy, S., Mitchell, M., Lins, R., 2007. Effect of renal impairment on the pharmacokinetics of exenatide. Br. J. Clin. Pharmacol. 64 (3), 317–327.
Lou, H., Hageman, M.J., 2022. Development of an In Vitro System To Emulate an In Vivo Subcutaneous Environment: Small Molecule Drug Assessment. Mol. Pharm. 19 (11), 4017–4025.
Lou, H., Berkland, C., Hageman, M.J., 2021. Simulating particle movement inside subcutaneous injection site simulator (SCISSOR) using Monte-Carlo method. Int. J. Pharm. 605, 120824.
Mach, H., Gregory, S.M., Mackiewicz, A., Mittal, S., Lalloo, A., Kirchmeier, M., Shameem, M., 2011. Electrostatic interactions of monoclonal antibodies with subcutaneous tissue. Ther. Deliv. 2 (6), 727–736.
Matuso, E.S., Tanaka, T., 1988. Kinetics of discontinous volume-phase transition of gels. J. Chem. Phys. 89, 1695–1703.
Mertz, N., Østergaard, J., Yaghmur, A., Larsen, S.W., 2019. Transport characteristics in a novel in vitro release model for testing the performance of intra-articular injectables. Int. J. Pharm. 566, 445–453.
Milewski, M., Manser, K., Nissley, B.P., Mitra, A., 2015. Analysis of the absorption kinetics of macromolecules following intradermal and subcutaneous administration. Eur. J. Pharm. Biopharm. 89, 134–144.
Nilsson, P., Hansson, P., 2005. Ion-exchange controls the kinetics of deswelling of polyelectrolyte microgels in solutions of oppositely charged surfactant. J. Phys. Chem. B 109, 23843–23856.
Nilsson, P., Hansson, P., 2007. Deswelling kinetics of polyacrylate gels in solutions of cetyltrimethylammunium bromide. J. Phys. Chem. B 111, 9770–9778.
Nilsson, P., Hansson, P., 2008. Regular and Irregular deswelling of polyacrylate and hyaluronate gels induced by oppositely charged surfactants. J. Colloid Int. Sci. 325, 316–323.
Parlow, J., Rodler, A., Gråsjö, J., Sjögren, H., Hansson, P., 2024. FRAP analysis of peptide diffusion in extracellular matrix mimetic hydrogels as an in vitro model for subcutaneous injection. Int. J. Pharm. 664, 124628.
Phillips-Jones, M.K., Lithgo, R., Dinu, V., Gillis, R.B., Harding, J.E., Adams, G.G., Harding, S.E., 2017. Full hydrodynamic reversibility of the weak dimerization of vancomycin and elucidation of its interaction with VanS monomers at clinical concentration. Sci. Rep. 7 (1), 12697.
Pieri, L., Wang, F., Arteni, A.-A., Vos, M., Winter, J.-M., Le Du, M.-H., Artzner, F., Gobeaux, F., Legrand, P., Boulard, Y., Bressanelli, S., Egelman, E.H., Paternostre, M., 2022. Atomic structure of Lanreotide nanotubes revealed by cryo-EM. Proc. Natl. Acad. Sci. 119 (4).
Podgornik, R., Åkesson, T., Jönsson, B., 1995. Colloidal interactions mediated via polyelectrolytes. J. Chem. Phys. 102, 9423–9434.
Pouget, E., Fay, N., Dujardin, E., Jamin, N., Berthault, P., Perrin, L., Pandit, A., Rose, T., Valéry, C., Thomas, D., Paternostre, M., Artzner, F., 2010. Elucidation of the Self-Assembly Pathway of Lanreotide Octapeptide into β-Sheet Nanotubes: Role of Two Stable Intermediates. J. Am. Chem. Soc. 132 (12), 4230–4241.
Rahimizadeh, P., Yang, S., Lim, S.I., 2020. Albumin: An Emerging Opportunity in Drug Delivery. Biotechnol. Bioprocess Eng. 25 (6), 985–995.
Reed, R.K., Lepsøe, S., Wiig, H., 1989. Interstitial exclusion of albumin in rat dermis and subcutis in over- and dehydration. Am. J. Phys. Anthropol. 257 (6 Pt 2), H1819–H1827.
Richter, W.F., Jacobsen, B., 2014. Subcutaneous absorption of biopharmaceutics: Knowns and unknowns. Drug Metab. Dispos. 42, 1881–1889.
Richter, W.F., Bhansali, S.G., Morris, M.E., 2012. Mechanistic determinants of biotherapeutics absorption following SC administration. AAPS J. 14 (3), 559–570.
Rodler, A., Samanta, A., Goh, W.-J., Hilborn, J., Hansson, P., 2024. Engineering and characterization of a hydrogel mimicking subcutaneous interstitial space. Eur. Polym. J. 205, 112739.
Sánchez-Félix, M., Burke, M., Chen, H.H., Patterson, C., Mittal, S., 2020. Predicting bioavailability of monoclonal antibodies after subcutaneous administration: Open innovation challenge. Adv. Drug Deliv. Rev. 167, 66–77.
Sasaki, S., Koga, S., Imabayashi, R., Maeda, H., 2001. Salt effects on the volume transition of ionic gel induced by the hydrophobic counterion binding. J. Phys. Chem. B 105, 5852–5855.
Schöner, T.A., Vogel, V., Venczel, M., Knoth, K., Kamm, W., Paehler, T., Louit, G., Terán, I.T., Mundinger, P., Marker, A., Loos, P., Hittinger, M., Lehr, C.-M., 2024. Biorelevant subcutaneous in vitro test predicts the release of human and fast acting insulin formulations. Int. J. Pharm. 655, 123995.
Shi, L., Wang, F., Zhu, W., Xu, Z., Fuchs, S., Hilborn, J., Zhu, L., Ma, Q., Wang, Y., Weng, X., Ossipov, D.A., 2017. Self-Healing Silk Fibroin-Based Hydrogel for Bone Regeneration: Dynamic Metal-Ligand Self-Assembly Approach. Adv. Funct. Mater. 27 (37), 1700591.
Singh-Franco, D., Robles, G., Gazze, D., 2007. Pramlintide acetate injection for the treatment of type 1 and type 2 diabetes mellitus. Clin. Ther. 29 (4), 535–562.
Skobeleva, V.B., Zinchenko, A.V., Rogacheva, V.B., Zezin, A.B., Kabanov, V.A., 2001. Interaction of hydrogels of acrylic acid-acrylamide copolymers with cytochrome c, Polymer Science. Ser. A 43 (3), 315–322.
Skovgaard, M., Kodra, J.T., Gram, D.X., Knudsen, S.M., Madsen, D., Liberles, D.A., 2006. Using Evolutionary Information and Ancestral Sequences to Understand the Sequence-Function Relationship in GLP-1 Agonists. J. Mol. Biol. 363 (5), 977–988.
Śliwińska-Hill, U., Wiglusz, K., 2020. The interaction between human serum albumin and antidiabetic agent - exenatide: determination of the mechanism binding and effect on the protein conformation by fluorescence and circular dichroism techniques - Part I. J. Biomol. Struct. Dyn. 38 (8), 2267–2275.
Song, J.Y., Larson, N.R., Thati, S., Torres-Vazquez, I., Martinez-Rivera, N., Subelzu, N.J., Leon, M.A., Rosa-Molinar, E., Schöneich, C., Forrest, M.L., Middaugh, C.R., Berkland, C.J., 2019. Glatiramer acetate persists at the injection site and draining lymph nodes via electrostatically-induced aggregation. J. Control. Release 293, 36–47.
Stace, T.M., Damiano, E.R., 2001. An electrochemical model of the transport of charged molecules through the capillary glycocalyx. Biophys. J . 80 (4), 1670–1690.
Stevenson, J., Poker, R., Schoss, J., Campbell, M., Everitt, C., Holly, B., Stones, N., Pettis, R.J., Sanchez-Felix, M., 2024. Pharmaceutical and biotech industry perspectives on optimizing patient experience and treatment adherence through subcutaneous drug delivery design. Adv. Drug Deliv. Rev. 209, 115322.
Tanaka, T., 1978. Collapse of gels and the critical endpoint. Phys. Rev. Lett. 40 (12), 820–823.
Thati, S., McCallum, M., Xu, Y., Zheng, M., Chen, Z., Dai, J., Pan, D., Dalpathado, D., Mathias, N., 2020. Novel Applications of an In Vitro Injection Model System to Study Bioperformance: Case Studies with Different Drug Modalities. J. Pharm. Innov. 15 (2), 268–280.
Torres-Terán, I., Venczel, M., Klein, S., 2021. Prediction of subcutaneous drug absorption - do we have reliable data to design a simulated interstitial fluid? Int. J. Pharm. 610, 121257.
Torres-Terán, I., Venczel, M., Stieler, T., Parisi, L., Kloss, A., Klein, S., 2023. Prediction of subcutaneous drug absorption - Characterization of subcutaneous interstitial fluids as a basis for developing biorelevant in vitro models. Int. J. Pharm. 638, 122906.
Trocóniz, I.F., Cendrós, J.M., Peraire, C., Ramis, J., Garrido, M.J., Boscani, P.F., Obach, R., 2009. Population pharmacokinetic analysis of lanreotide Autogel in healthy subjects : evidence for injection interval of up to 2 months. Clin. Pharmacokinet. 48 (1), 51–62.
Varkhede, N., Bommana, R., Schöneich, C., Forrest, M.L., 2020. Proteolysis and Oxidation of Therapeutic Proteins After Intradermal or Subcutaneous Administration. J. Pharm. Sci. 109 (1), 191–205.
Viola, M., Sequeira, J., Seiça, R., Veiga, F., Serra, J., Santos, A.C., Ribeiro, A.J., 2018. Subcutaneous delivery of monoclonal antibodies: How do we get there? J. Control. Release 286, 301–314.
Wanselius, M., Rodler, A., Searle, S.S., Abrahmsén-Alami, S., Hansson, P., 2022. Responsive Hyaluronic Acid - Ethylacrylamide Microgels Fabricated Using Microfluidics Technique. Gels 8 (9), 588.
Wanselius, M., Searle, S., Rodler, A., Tenje, M., Abrahmsén-Alami, S., Hansson, P., 2022. Microfluidics platform for studies of peptide – polyelectrolyte interaction. Int. J. Pharm. 621, 121785.
Wanselius, M., Al-Tikriti, Y., Hansson, P., 2023. Utilizing a microfluidic platform to investigate drug-eluting beads: Binding and release of amphiphilic antidepressants. Int. J. Pharm. 647, 123517.
Wiig, H., Swartz, M.A., 2012. Interstitual fluid and lymph formation and transport: Physiological regulation and roles in inflammation and cancer. Physiol. Rev. 92, 1005–1060.
Zezin, A.B., Rogacheva, V., Skobeleva, V., Kabanov, V., 2002. Controlled uptake and release of proteins by polyelectrolyte gels. Polym. Adv. Technol. 13, 919–925.